

# A Pervasively Correlated Channel Model for Massive MIMO Transmission

Min Wang, *Member, IEEE*, Yaping He, Haiming Wang, *Member, IEEE*,  
Cheng-Xiang Wang, *Fellow, IEEE*, and Xiaohu You, *Fellow, IEEE*

**Abstract**—The statistical gap between existing correlation-based stochastic channel models (CBSMs) and practical propagation is a longstanding issue, especially for massive multiple-input multiple-output (MIMO) transmission. To address this problem, a pervasively correlated channel model (PCCM) applicable to MIMO channels with arbitrary antenna configurations and scenarios is proposed. Unlike the conventional jointly correlated channel model (JCCM) based on an independently and identically distributed (i.i.d.) random matrix, a new random matrix whose elements are independent and nonidentically distributed (i.n.d.) generalized Gamma complex Gaussian mixture (GGCGM) variables with correlated envelopes is used to approximate the real channel statistics better. Moreover, the PCCM can be simplified via the Rayleigh fading assumption for rapid evaluation of channel performance and supports backward compatibility with existing CBSMs under specific assumptions. Demonstrative numerical experiments for MIMO channels are conducted based on the 3GPP TR 38.901 model considering various scenarios, frequencies, and antenna configurations. The channel capacity distributions are obtained based on random samples generated using the geometry-based stochastic channel model (GBSM), the JCCM, and the proposed PCCM. The numerical results show that the PCCM is more flexible than the JCCM with respect to high-order statistics, enabling more accurate estimation of massive MIMO transmission channel performance.

**Index Terms**—Channel modeling, multiple-input multiple-output (MIMO), massive MIMO, correlation-based stochastic channel model (CBSM), channel capacity, spatial correlation, channel statistical properties.

## I. INTRODUCTION

**T**HE massive multiple-input multiple-output (MIMO) transmission has been recognized as a key technology

Manuscript received June 2, 2023; revised Oct. 7, 2023; accepted Dec. 9, 2023. Date of publication ; date of current . This work was supported in part by the National Key R&D Program of China under Grant 2020YFB1804901, the National Natural Science Foundation of China under Grants 62271133 and 61960206006, and the Keysight's University Research Collaborations program. (*Corresponding author: Haiming Wang*)

M. Wang and Y. P. He are with the Pervasive Communication Research Center, Purple Mountain Laboratories, Nanjing 211111, China (e-mail: wangmin@pmlabs.com.cn; he\_cloris@163.com).

H. M. Wang is with the State Key Laboratory of Millimeter Waves, Southeast University, Nanjing 210096, China, and also with the Pervasive Communication Research Center, Purple Mountain Laboratories, Nanjing 211111, China (e-mail: hmwang@seu.edu.cn).

C. X. Wang and X. H. You are with the National Mobile Communications Research Laboratory, Southeast University, Nanjing 210096, China, and also with the Pervasive Communication Research Center, Purple Mountain Laboratories, Nanjing 211111, China (e-mail: chxwang@seu.edu.cn; xhyu@seu.edu.cn).

Color versions of one or more of the figures in this paper are available online at <http://ieeexplore.ieee.org>.

Digital Object Identifier

to increase the array gain and degrees of freedom for spatial multiplexing in future wireless communications [1]–[6]. As the most intuitive feature of channel performance, substantial attention has been drawn in recent years to studying the MIMO channel capacity associated with the transmission scheme and multipath richness [7]–[10]. With channel characteristics acquired through channel measurements, the multipath transmission coefficients can be represented by mathematical expressions, i.e., channel modeling. Considering the significant workload and cost of the channel measurement campaign, a reliable channel model is of great importance for the arrangement, evaluation and optimization of the communication system.

There are two mainstream channel modeling methods in the literature, i.e., the stochastic-based model and the deterministic model [11], [12]. In particular, the stochastic-based channel model [13]–[16] uses a set of random input variables for each channel implementation and is commonly used to obtain the statistical properties of the link- and system-level channel, while the deterministic model [17] uses fixed inputs to simulate the realistic signal propagation process.

In this work, we focus on the stochastic-based channel model, which can be further divided into two categories: the geometry-based stochastic channel model (GBSM) and the correlation-based stochastic channel model (CBSM). A GBSM is considered relatively accurate compared to a CBSM since it is derived based on the fundamental laws of wave propagation with a predefined distribution of random scatterers [18]–[21]. Therefore, recent official standard channel models, such as the 3rd Generation Partnership Project spatial channel model (3GPP SCM) [22], the International Telecommunication Union Wireless World Initiative for New Radio II (ITU WINNER II) model [23] and the European Cooperation in Science and Technology 2100 (COST 2100) channel model, are commonly proposed with GBSMs. However, the implementation complexity of the GBSM makes it difficult for further use in analytical operations.

To overcome this drawback, CBSMs with concise expressions for statistical channel properties that are more applicable for signal processing research and channel performance evaluation have been proposed. The simplest CBSMs are Rayleigh, Rice, and Nakagami-m fading channel models for single-input single-output (SISO) wireless communications, which are used to characterize the statistical properties of the signal envelope. However, they are not applicable for correlated MIMO channels. Assuming the spatial correlation properties at both link ends are independent of each other, the Kronecker-

based channel model (KBSM) was proposed in [24]. On this basis, a number of studies have addressed the relationship between the MIMO channel performance and spatiotemporal correlation [25]–[28].

Nevertheless, studies clearly indicate that the KBSM cannot fit well into the practical channel due to its excessive simplification of the spatial correlation model. Considering joint correlations over MIMO channels, [29] presented a virtual channel representation (VCR) that provides an insightful imaging interpretation of the scattering geometry. However, this representation supports MIMO links with only single polarized uniform linear arrays (ULAs). Inspired by the KBSM and VCR, the primary jointly correlated channel model (JCCM), i.e., Weichselberger’s model, was proposed in [30] for non-line-of-sight (NLOS) MIMO channels that consider both the mutual correlation and coupling between both link ends, but this approach has limitations in that the independent random elements in the model are complex Gaussian variables and the line-of-sight (LOS) components are not embodied in the expression. These restrictions were further liberalized in the jointly correlated channel model (JCCM) formula [31], where a determined LOS coupling matrix was introduced and the normalized random elements were still independently distributed but no longer restricted to a Gaussian shape. On this basis, the closed-form upper-bound expression of the ergodic capacity based on statistical eigenmode transmission was derived. However, the JCCM still assumes that the independent channel coefficients are identically distributed, which may cause deviations from reality, and the distortion can be even worsen along with the growth of the MIMO antenna scale. In view of the increasing application of massive MIMO antennas in communication systems, developing a CBSM with high accuracy in statistics for massive MIMO transmission has become an urgent issue.

Two schemes transformed from the CBSM that apply to massive MIMO channels have been discussed in the literature. Based on Monte Carlo (MC) simulation, a Gamma distribution-based eigenvalue (EV) model associated with the transmitting and receiving correlation properties was proposed in [32], [33], which makes the prediction of the channel capacity more convenient. However, this model cannot be transformed to existing CBSMs representing the channel matrix and supports only a  $2 \times N$  or  $N \times 2$  MIMO channel. The other scheme is an integration of the GBSM and CBSM. A typical example is presented in [21], [34], where the beam domain channel model (BDCM) is introduced in the JCCM as a substitute for the random matrix. This model applies the physical fundamentals of the GBSM, which improves the JCCM accuracy for massive MIMO channels while somewhat increasing the complexity of modeling. In addition, the BDCM is proposed based on the massive MIMO assumption, which means performance degradation for small-scale MIMO communication scenarios.

In summary, there is a clear demand for a more general CBSM with both low structural complexity and high statistical accuracy for massive MIMO transmission. To address this need, a pervasively correlated channel model (PCCM) is proposed in this paper; the approach is pervasively appli-

cable to arbitrary antenna configurations and scenarios. The proposed channel model has been demonstrated to provide a perfect statistical approximation to the 3GPP TR 38.901 channel model [35], a widely recognized GBSM standard. The contributions of this study are summarized as follows:

- 1) The statistical properties of jointly correlated MIMO channels are investigated in detail, aiming to elucidate the distortions encountered in conventional JCCM;
- 2) An independent and nonidentically distributed (i.n.d.) random matrix, which comprises entries that follow a multidimensional generalized Gamma complex Gaussian mixture (GGCGM) distribution, is proposed;
- 3) On this basis, a novel CBSM termed PCCM, which has versatile applicability in MIMO channels with arbitrary antenna configurations and scenarios, is presented. The random entries exhibit correlated magnitudes and independent phase components, rendering it a suitable tool for accurately modeling stochastic MIMO channel coefficients;
- 4) The PCCM is compatible with existing CBSMs. Additionally, two reduced variants, i.e., the simplified PCCM (SCCM) and the generalized JCCM (GCCM), are also proposed for efficient parameterization and analytical analysis;
- 5) Notably, the PCCM boasts a concise framework and exceptional statistical accuracy. These attributes position it as an efficient and dependable tool for channel characterization and transmission design for massive MIMO communication.

The rest of this paper is organized as follows. First, the fundamentals of MIMO communications over jointly correlated MIMO channels are given in Section II. On this basis, a new JCCM named PCCM is then proposed in Section III with a detailed parameterization method. Finally, to verify the proposed model, Section IV presents a series of numerical experiments of MIMO channels with various scenarios, frequencies and antenna configurations, as well as comparisons of the channel performance based on the GBSM, JCCM and PCCM.

*Notation:* The following notation is adopted throughout this paper. We use upper (lower) bold-face letters to denote matrices (vectors). The subscripts  $t$  and  $r$  indicate the transmitter and receiver sides, respectively.  $\mathbf{I}_{M \times M}$  represents an identity matrix of size  $M \times M$ .  $\text{diag}\{\cdot\}$  means outputting a diagonal matrix with the elements of a vector on the main diagonal. The vectorization of an  $M \times N$  matrix  $\mathbf{A}$ , denoted  $\text{vec}(\mathbf{A})$ , is the  $MN \times 1$  column vector obtained by stacking the columns of the matrix  $\mathbf{A}$  on top of one another.  $(\cdot)^T$ ,  $(\cdot)^*$ , and  $(\cdot)^H$  are the transpose, conjugate and conjugate-transpose operations, respectively.  $\odot$  represents the matrix dot product, and  $\otimes$  represents taking the Kronecker product. Operations  $\mathbb{E}\{\cdot\}$ ,  $\text{Var}\{\cdot\}$  and  $\text{Kr}\{\cdot\}$  are, respectively, defined as taking the expectation, variance and kurtosis of a random variable or matrix elements. The rank and trace of a matrix are indicated by  $\text{rank}\{\cdot\}$  and  $\text{tr}\{\cdot\}$ , respectively.

## II. FUNDAMENTALS OF MIMO TRANSMISSION

### A. Signal Model

Without loss of generality, a single-user link system over a frequency-flat time-varying MIMO fading channel with  $M$

transmit (Tx) and  $N$  receive (Rx) antennas is considered. The  $M \times N$  MIMO channel matrix is denoted as  $\mathbf{H}$ , in which the element  $[\mathbf{H}]_{m,n}$  is the channel gain from the  $n$ th Tx antenna to the  $m$ th Rx antenna. Then, the  $N \times 1$  received signal vector in a single symbol interval can be modeled as:

$$\mathbf{y} = \mathbf{H}\mathbf{x} + \mathbf{z} \quad (1)$$

where  $\mathbf{x} \in \mathbb{C}^{M \times 1}$  represents the transmit complex signal vector and  $\mathbf{z} \in \mathbb{C}^{N \times 1}$  is the additive white Gaussian noise (AWGN) vector at the receiving end with covariance matrix  $\sigma_z^2 \mathbf{I}_{N \times N}$ .

Assuming that the  $\mathbf{x}$  sequences are independent and identically distributed (i.i.d.) complex Gaussian entries, the average transmit signal power is:

$$\mathbb{E} \{ \text{tr} \{ \mathbf{x}\mathbf{x}^H \} \} = P_t \quad (2)$$

where  $P_t$  is the total transmit signal power. Particularly, if uniform power allocation is employed, we have

$$\mathbb{E} \{ \mathbf{x}\mathbf{x}^H \} = \frac{P_t}{M} \mathbf{I}_{M \times M}. \quad (3)$$

The singular value decomposition (SVD) of the channel matrix reads as

$$\mathbf{H} = \mathbf{U}\mathbf{\Sigma}\mathbf{V}^H \quad (4)$$

where  $\mathbf{U} \in \mathbb{C}^{N \times \text{rank}\{\mathbf{H}\}}$  and  $\mathbf{V} \in \mathbb{C}^{M \times \text{rank}\{\mathbf{H}\}}$  are unitary matrices and  $\mathbf{\Sigma}$  is the diagonal matrix of the nonzero singular values (SVs) of  $\mathbf{H}$ , i.e.,

$$\mathbf{\Sigma} = \text{diag} \{ [\varepsilon_1, \varepsilon_2, \dots, \varepsilon_{\text{rank}\{\mathbf{H}\}}] \}. \quad (5)$$

In theory, via SVD-based multiplexing, the MIMO channel can be decomposed into  $\text{rank}\{\mathbf{H}\}$  parallel and independent SISO subchannels. We recall that a unitary matrix  $\mathbf{U}$  satisfies  $\mathbf{U}\mathbf{U}^H = \mathbf{U}^H\mathbf{U} = \mathbf{I}$ , and we have the eigenvalue decomposition (EVD) of  $\mathbf{H}\mathbf{H}^H$  given by:

$$\mathbf{H}\mathbf{H}^H = \mathbf{U}\mathbf{\Lambda}\mathbf{U}^H \quad (6)$$

where  $\mathbf{\Lambda}$  is a rectangular matrix whose diagonal elements are the ordered positive real EVs of the MIMO channel:

$$\mathbf{\Lambda} = \mathbf{\Sigma}\mathbf{\Sigma}^H = \text{diag} \{ [\lambda_1, \lambda_2, \dots, \lambda_{\text{rank}\{\mathbf{H}\}}] \}. \quad (7)$$

Thus, the MIMO channel power gain can be obtained:

$$G = \text{tr} \{ \mathbf{H}\mathbf{H}^H \} = \sum_{i=1}^{\text{rank}\{\mathbf{H}\}} \lambda_i. \quad (8)$$

Then, the average signal-to-noise ratio (SNR) per Rx antenna can be estimated as

$$\text{SNR}_{\text{avg}} = \frac{GP_t}{N\sigma_z^2} = \frac{\text{tr} \{ \mathbf{H}\mathbf{H}^H \} P_t}{N\sigma_z^2}. \quad (9)$$

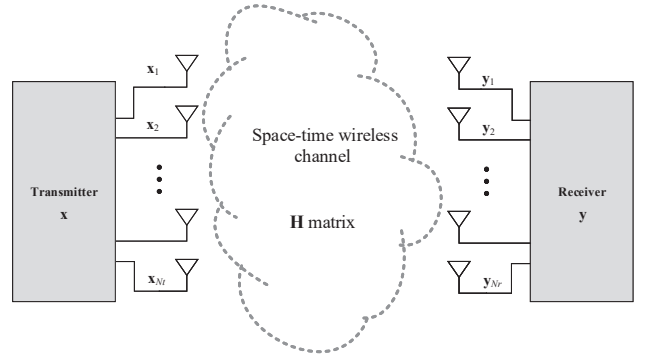


Fig. 1. Diagram of a wireless MIMO channel.

### B. Jointly Correlated MIMO Channels

The structure of a wireless MIMO channel is represented schematically in Fig. 1. The channel spatial behavior can be represented by the full correlation matrix of  $\mathbf{H}$  defined below, including the joint correlation properties of both link sides.

$$\mathbf{R}_{\mathbf{H}} \triangleq \mathbb{E} \{ \text{vec}(\mathbf{H}) \text{vec}(\mathbf{H})^H \}. \quad (10)$$

However, the full correlation matrix is not recommended for channel modeling since it has massive entries to be specified. As a special case, an i.i.d. Gaussian-distributed  $\mathbf{H}$  can be fully characterized by its full correlation matrix, while this strict condition is rare to achieve in reality.

Previous research [29] has noted that the joint correlation properties over the wireless MIMO channel are key characteristics of the MIMO channel that cannot be omitted in rigorous channel modeling. Thus, the expression of the one-sided correlation matrices should consider the statistical signal properties of the other link end, as given below:

$$\begin{cases} \mathbf{R}_{\mathbf{t}, \mathbf{Q}_t} \triangleq \mathbb{E} \{ \mathbf{H}^H \mathbf{Q}_t \mathbf{H} \}, \\ \mathbf{R}_{\mathbf{r}, \mathbf{Q}_r} \triangleq \mathbb{E} \{ \mathbf{H} \mathbf{Q}_r \mathbf{H}^H \}. \end{cases} \quad (11)$$

where  $\mathbf{Q}_t$  and  $\mathbf{Q}_r$  are the spatial signal covariance matrices at the transmitter and receiver sides, respectively.

To further simplify, considering a spatial multiplexing transmission, in theory, a reasonable approximation can be made that the signal covariance of the other link is spatially white. On this basis, the transmit and receive correlation matrices are established as:

$$\begin{cases} \mathbf{R}_t \triangleq \mathbb{E} \{ \mathbf{H}^H \mathbf{H} \} = \mathbf{U}_t \mathbf{\Lambda}_t \mathbf{U}_t^H \\ \mathbf{R}_r \triangleq \mathbb{E} \{ \mathbf{H} \mathbf{H}^H \} = \mathbf{U}_r \mathbf{\Lambda}_r \mathbf{U}_r^H \end{cases} \quad (12)$$

where  $\mathbf{U}_t$ ,  $\mathbf{U}_r$  and  $\mathbf{\Lambda}_t$ ,  $\mathbf{\Lambda}_r$  are the eigenbases and the diagonal matrices consisting of the eigenvalues of  $\mathbf{R}_t$ ,  $\mathbf{R}_r$ , respectively.

With the above assumption, the spatial eigenbases  $\mathbf{U}_t$  and  $\mathbf{U}_r$  are independent of the signal correlation, which lays the foundation for the JCCM development:

$$\mathbf{H}_{\text{Model}} = \mathbf{U}_r \tilde{\mathbf{H}} \mathbf{U}_t^H \quad (13)$$

where  $\tilde{\mathbf{H}}$  is a random matrix with independent elements.

### III. Pervasively Correlated Channel Model

#### A. PCCM Formula

As in (13), the statistics of the MIMO wireless channel consist of three parts: the eigenbasis matrices  $\mathbf{U}_r$  and  $\mathbf{U}_t$ , which reflect the spatial correlation of the MIMO channel depending on the transmit and receive antenna configurations, and a random matrix  $\tilde{\mathbf{H}}$ , which statistically characterizes the realistic propagation environments.

It is easy to find that  $\tilde{\mathbf{H}}$  dominates the random properties of the MIMO channel without spatial correlation. On this basis, we have the mathematical fundamental for eigenmode transmission:

$$\tilde{\mathbf{H}} = \mathbf{U}_r^H \mathbf{H} \mathbf{U}_t. \quad (14)$$

In the JCCM [31], the matrix  $\tilde{\mathbf{H}}$  is further divided into determined LOS and random NLOS components and a random matrix  $\mathbf{H}_{\text{id}}$  with i.i.d. elements, which are assumed to be the normalized NLOS  $\tilde{\mathbf{H}}$  coefficient and reflect the diversity of each independent subchannel. However, due to the strict precondition of identical distribution, the higher-order statistics represented by the JCCM may differ from physical reality for correlated MIMO channels. In addition, the distortion worsens with increasing MIMO scale and spatial correlation, thereby leading to significant deviations of the channel performance for massive MIMO transmission.

To achieve a better approximation of the real channel properties, we propose a new CBSM, named PCCM, for massive MIMO channels, which is pervasively applicable to arbitrary scenarios and antenna configurations. The PCCM proceeds to use the classic JCCM structure framework. The formula is given below:

$$\begin{aligned} \mathbf{H}_{\text{PCCM}} &= \mathbf{U}_r \tilde{\mathbf{H}} \mathbf{U}_t^H \\ &= \mathbf{U}_r \left( \tilde{\mathbf{D}} + \tilde{\mathbf{M}} \odot \mathbf{H}_{\text{id}} \right) \mathbf{U}_t^H. \end{aligned} \quad (15)$$

Compared with conventional JCCMs, the new model has a similar structure with some changes made to the definitions of partial parameters: the elements  $\mathbf{U}_r$ ,  $\mathbf{U}_t$  and  $\mathbf{H}_{\text{id}}$  have the same definitions as those in the JCCM. The difference is that the LOS and NLOS coupling matrices in the PCCM, i.e.,  $\tilde{\mathbf{D}}$  and  $\tilde{\mathbf{M}}$ , consist of  $N \times M$  independent random nonnegative entries.

#### B. PCCM Parameterizations

The matrices  $\tilde{\mathbf{D}}$  and  $\tilde{\mathbf{M}}$  reflect the LOS and NLOS scattering components of the channel, respectively. Once the LOS component is determined, (15) can be further concretized as

$$\begin{aligned} \mathbf{H}' &= \mathbf{U}_r \tilde{\mathbf{H}} \mathbf{U}_t^H \\ &= \mathbf{U}_r \left( \mathbf{D} + \mathbf{M} \odot \mathbf{H}_{\text{ind}} \right) \mathbf{U}_t^H. \end{aligned} \quad (16)$$

where  $\mathbf{D}$  and  $\mathbf{M}$  are  $N \times M$  deterministic real matrices and  $\mathbf{H}_{\text{ind}}$  represents an  $N \times M$  random matrix with i.n.d. entries.

This model divides the representation of the entire channel into two parts: the correlation arising from the transceiver antennas and the transmission coefficients within the air-interface channel after eliminating antenna-related effects. Notably, in contrast to JCCM, this model takes into account

the correlation of the propagation envelopes induced by the propagation environment.

All the parameters can be extracted from channel samples obtained from either practical measurements or Monte Carlo (MC) simulations. First, one must obtain the small-scale channel coefficients  $\mathbf{H}_{\text{SS}}$  by normalizing the raw data set of the channel impulse responses  $\mathbf{H}$ :

$$\mathbf{H}_{\text{SS}} = \frac{\mathbf{H}_{\text{raw}}}{\beta_{\text{LS}}} \quad (17)$$

where  $\beta_{\text{LS}}$  denotes the large-scale channel path gain between the BS and the UE.

The unitary matrices  $\mathbf{U}_r$  and  $\mathbf{U}_t$  can be obtained based on the EVDs of the transmit and receive channel correlation matrices as (12), respectively. After removing the spatial correlations of the MIMO channel with the eigenbases  $\mathbf{U}_r$  and  $\mathbf{U}_t$ , the resulting matrix  $\tilde{\mathbf{H}}$  reflects the practical statistical behavior of the multipath propagation,

$$\tilde{\mathbf{H}} = \mathbf{U}_r^H \mathbf{H}_{\text{SS}} \mathbf{U}_t. \quad (18)$$

On the premise that the deterministic matrices  $\mathbf{D}$  and  $\mathbf{M}$  are, respectively, given by

$$\mathbf{D} = \mathbb{E} \left\{ \tilde{\mathbf{H}} \right\} \quad (19)$$

$$[\mathbf{M}]_{m,n} = \sqrt{\text{Var} \left\{ [\tilde{\mathbf{H}}]_{m,n} \right\}} = \sqrt{\text{Var} \left\{ [\mathbf{H}_{\text{SS}}]_{m,n} - [\mathbf{D}]_{m,n} \right\}}. \quad (20)$$

The elements of the random matrix  $\mathbf{H}_{\text{ind}}$  statistically represent the normalized elements of  $\tilde{\mathbf{H}}$ .

The key to accurately representing the channel characteristics is to find proper probability distributions for the elements of matrix  $\mathbf{H}_{\text{ind}}$ . Unlike previous CBSMs that model the random matrix with defined distributions for its real and imaginary (R/I) parts, potentially ignoring correlations between the magnitudes and phases of individual elements, we adopt a different approach. Specifically, we assume that the entries of  $\mathbf{H}_{\text{ind}}$  are represented using an alternative representation, namely, the magnitude and phase representation, which enables the capture of more statistical characteristics. The corresponding expression is given below:

$$\mathbf{H}_{\text{ind}} = \mathbf{A}_{\text{cnd}} \odot \exp(j\mathbf{P}_{\text{id}}) \quad (21)$$

where  $\mathbf{A}_{\text{cnd}}$  represents the amplitude components of  $\mathbf{H}_{\text{ind}}$  and consists of correlated and nonidentical generalized Gamma entries, whereas  $\mathbf{P}_{\text{id}}$  is the phase matrix, whose i.i.d. elements are uniformly distributed within  $[-\pi, \pi]$ .

Since the operations on Gamma variables do not possess linearity invariance, it is not feasible to directly generate a multidimensional Gamma variable (MGV) with specific correlation properties. Nevertheless, generating a multivariate normal distribution proves to be more convenient. Therefore, a distribution transformation approach wherein correlated Gamma variables are generated with the cumulative probabilities of correlated standard Gaussian variables is proposed, providing control over the statistical properties of the target MGV. The detailed scheme is outlined below.

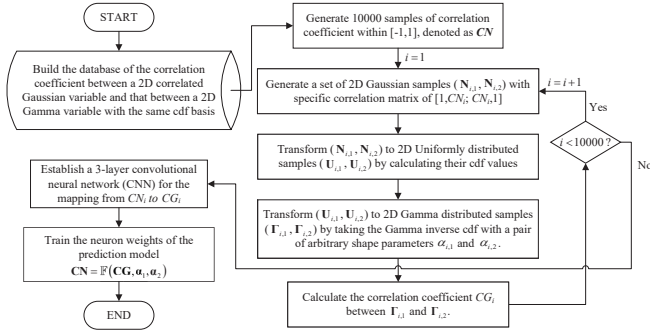


Fig. 2. Flowchart of establishing the predictive model.

- (1) Fit the magnitude of  $[\mathbf{H}_{\text{ind}}]_{m,n}$  to a generalized Gamma distribution, notated as

$$[\mathbf{A}_{\text{cnd}}]_{m,n} = \left| [\mathbf{H}_{\text{ind}}]_{m,n} \right| \sim \Gamma(\alpha_{m,n}, \beta_{m,n}, \gamma_{m,n}, 0). \quad (22)$$

- (2)  $\left| [\mathbf{H}_{\text{ind}}]_{m,n} \right|$  is transformed into a Gamma distribution:

$$[\mathbf{A}'_{\text{cnd}}]_{m,n} = \left\{ \left| [\mathbf{H}_{\text{ind}}]_{m,n} \right| \right\}^{\gamma_{m,n}} \sim \Gamma(\alpha_{m,n}, \beta_{m,n}, 1, 0). \quad (23)$$

- (3) Calculate the full correlation matrix of  $\mathbf{A}'_{\text{cnd}}$ :

$$\mathbf{R}_{\mathbf{A}'_{\text{cnd}}} = \mathbb{E} \left\{ \text{vec}(\mathbf{A}'_{\text{cnd}}) \text{vec}(\mathbf{A}'_{\text{cnd}})^{\text{H}} \right\}. \quad (24)$$

- (4) Calculate the full correlation matrix  $\mathbf{R}_{\text{MNVs}}$  of the multidimensional normal variable (MNV) mapped to  $\mathbf{R}_{\mathbf{A}'_{\text{cnd}}}$ . Due to the challenge of deriving an analytical solution for mapping correlation coefficients between Gamma variables to those between Gaussian variables, a machine learning predictive model is constructed, as depicted in Fig. 2.
- (5) MNV samples are generated using the specified full correlation matrix  $\mathbf{R}_{\text{MNVs}}$  and are transformed into MGv samples (i.e.,  $\mathbf{A}'_{\text{cnd}}$ ) following Appendix A.
- (6) Corresponding  $\mathbf{A}_{\text{cnd}}$  samples are restored through the operation below:

$$[\mathbf{A}_{\text{cnd}}]_{m,n} = [\mathbf{A}'_{\text{cnd}}]_{m,n}^{1/\gamma_{m,n}}. \quad (25)$$

By this point, all the parameters in the PCCM are initialized. The distance between the statistical properties of the PCCM and GBSM samples can be efficiently evaluated in terms of the multidimensional KLD between the EVs obtained from the raw channel coefficients  $\mathbf{H}_{\text{raw}}$  and the replicated samples generated by the PCCM:

$$\begin{aligned} \Delta &= D_{\text{KL}} \left( p_{\Lambda_{\text{H}_{\text{SS}}} \parallel q_{\Lambda_{\text{H}'_{\text{SS}}}} \right) + D_{\text{KL}} \left( q_{\Lambda_{\text{H}'_{\text{SS}}} \parallel p_{\Lambda_{\text{H}_{\text{SS}}} \right) \\ &= \sum_{l=1}^L \left[ p_{\Lambda_{\text{H}_{\text{SS}}}(\mathbf{X}_l) \ln \left( \frac{p_{\Lambda_{\text{H}_{\text{SS}}}(\mathbf{X}_l)}{q_{\Lambda_{\text{H}'_{\text{SS}}}(\mathbf{X}_l)}} \right) \right. \\ &\quad \left. + q_{\Lambda_{\text{H}'_{\text{SS}}}(\mathbf{X}_l) \ln \left( \frac{q_{\Lambda_{\text{H}'_{\text{SS}}}(\mathbf{X}_l)}{p_{\Lambda_{\text{H}_{\text{SS}}}(\mathbf{X}_l)}} \right) \right] \end{aligned} \quad (26)$$

where  $p_{\Lambda_{\text{H}_{\text{SS}}}}$  and  $q_{\Lambda_{\text{H}'_{\text{SS}}}}$  represent the joint probability functions of the PCCM and practical EVs, respectively.

### C. Backward Compatibility of the PCCM

The PCCM offers a versatile framework for achieving compatibility with various existing CBSMs through specified shape and scale parameters. This adaptability arises from the transformation of a generalized Gamma variable into distributions such as Rayleigh, Rice, or Nakagami-m. In this section, we elaborate on the key points illustrating how PCCM establishes compatibility.

- 1) JCCM Simplification ( $\mathbf{A}_{\text{cnd}}$  Independence): Under the assumption that  $\mathbf{A}_{\text{cnd}}$  consists of i.i.d. elements, the PCCM formula reduces to the classical JCCM [31];
- 2) Weichselberger's Model Derivation: By degenerating all  $\mathbf{H}_{\text{ind}}$  elements to complex Gaussian variables and under the premise that  $\mathbf{D} = 0$ , Weichselberger's model [30] is obtained;
- 3) Kronecker Model for Separable-Correlated NLOS MIMO Channels: On the basis of (2), if the spatial correlations between the transmitting and receiving ends are neglected, the PCCM can be further reduced to a Kronecker model [27] for separable-correlated NLOS MIMO channels;
- 4) Transformation of Earlier CBSMs: With some additional preconditions of the channel properties, even earlier CBSMs can be transformed from the PCCM framework. Such transformations have been discussed in published works [30], [31] and are not elaborated on here.

By neglecting the correlation properties between the elements of  $\mathbf{A}_{\text{cnd}}$ , the PCCM can be simplified to a generalized JCCM (GCCM) with the matrix  $\mathbf{H}_{\text{ind}}$  consisting of i.n.d. GGCGM entries (Appendix B), which can be further expressed as:

$$\mathbf{H}_{\text{ind}} = \mathbf{R}_{\text{ind}} \odot \mathbf{G}_{\text{iid}} \quad (27)$$

where the elements of the random matrices  $\mathbf{G}_{\text{iid}}$  and  $\mathbf{R}_{\text{ind}}$  are independent of each other. Specifically, the elements of the matrix  $\mathbf{G}_{\text{iid}}$  are restricted to obey a standard complex Gaussian distribution, while the elements of the matrix  $\mathbf{R}_{\text{ind}}$  are i.n.d. power-generalized Gamma variables, i.e.,

$$[\mathbf{H}_{\text{ind}}]_{m,n} = r_{m,n}^{p_{m,n}} g_{m,n} \quad (28)$$

where  $r_{m,n} \sim \Gamma(\alpha_{m,n}, \beta_{m,n}, \Gamma_{m,n}, \mu_{m,n})$  and  $g_{m,n}$  denotes a standard complex Gaussian variable.

According to the definition of the GGCGM distribution, by taking different values of  $p_{m,n}$ , the elements of  $\mathbf{H}_{\text{ind}}$  can be transformed into complex Gaussian-distributed, complex Student-distributed or near-complex Laplace-distributed variables. Thus, the GCCM is compatible with the JCCM and Weichselberger's model.

Another simplification of the PCCM can be achieved by assuming the elements of  $\mathbf{H}_{\text{ind}}$  to be identically distributed, i.e., substituting  $\mathbf{A}_{\text{cnd}}$  with  $\mathbf{A}_{\text{cid}}$  consisting of correlated and identical Rayleigh-distributed entries, which is more tractable for mathematical analysis. The realization of  $\mathbf{A}_{\text{cid}}$  is similar to the MGv generation scheme. To distinguish it from the GCCM, we refer to this model as the simplified PCCM (SCCM). The SCCM degrades to the JCCM when the correlation properties of the elements of  $\mathbf{A}_{\text{cid}}$  are neglected.

Taken together, the i.n.d.  $\mathbf{H}_{\text{ind}}$  elements have more statistical degrees of freedom than do the i.i.d. random elements in the

existing JCCMs, making the PCCM more general and accurate in representing MIMO channels with arbitrary scenarios and MIMO scales. The PCCM formula can statistically represent the wireless MIMO channels of the following situations:

- 1) The stochastic LOS/NLOS MIMO channels at the cluster level, which means constant base station and user terminal (BS/UE) locations, antenna orientations, cluster positions and random scatters within a cluster;
- 2) Stochastic LOS/NLOS MIMO channels with constant BS/UE locations, antenna orientations and K factor but random multipath scattering;
- 3) The continuous time evolution of NLOS MIMO channels, which indicates time-varying arrival angles, cluster and subpath offsets;
- 4) The stochastic NLOS MIMO channels for multiple users that are uniformly dropped in a cell.

#### D. Channel Capacity

To facilitate evaluating the performance of MIMO channels of different scales, the eigenvalues decomposed from  $\mathbf{H}\mathbf{H}^H$  are normalized to the mean power of all the subchannel coefficients between each pair of single Tx and single Rx antennas, i.e.,

$$\bar{\lambda}_k = \frac{MN\lambda_k}{\mathbb{E} \left\{ \sum_{m=1}^M \sum_{n=1}^N \left| [\mathbf{H}]_{m,n} \right|^2 \right\}} \quad (29)$$

where  $k = 1, 2, \dots, \text{rank} \{ \mathbf{H} \}$ .

Assuming the transmitter has no knowledge of the CSI, the narrowband MIMO channel capacity can be expressed as

$$C = \log_2 \det \left( \mathbf{I}_{N \times N} + \frac{\text{SNR}_{\text{avg}}}{M} \mathbf{H}\mathbf{H}^H \right) \quad [\text{bps/Hz}]. \quad (30)$$

With uniform power allocation at the transmit end, the normalized channel capacity is given based on eigenvalue characteristics:

$$\bar{C} = \sum_{k=1}^{\text{rank}(\mathbf{H})} \log_2 \left( 1 + \frac{\bar{\lambda}_k P_t}{M \sigma_z^2} \right) \quad [\text{bps/Hz}]. \quad (31)$$

#### IV. NUMERICAL RESULTS AND ANALYSIS

The latest 3GPP channel model for the full frequency range from 0.5 GHz to 100 GHz, covering the entire frequency spectrum from 0.5 GHz to 100 GHz and encompassing definitions and specifications of geometric channel parameters for various scenarios, is detailed in 3GPP TR 38.901, which is hereinafter called the 3GPP 38.901 model. This model is widely regarded as a standard GBSM for link- and system-level channel simulations. However, it is crucial to emphasize that the 3GPP 38.901 model achieves perfect channel representation performance at the expense of implementation simplicity.

To verify the proposed PCCM, the 3GPP 38.901 model is adopted for a series of MIMO channel simulations based on the quasideterministic radio channel generator (QuaDRiGa) platform with various scenarios, frequencies and MIMO antenna configurations. For simplicity, only outdoor users are considered in the experiments, all the transceiver antennas

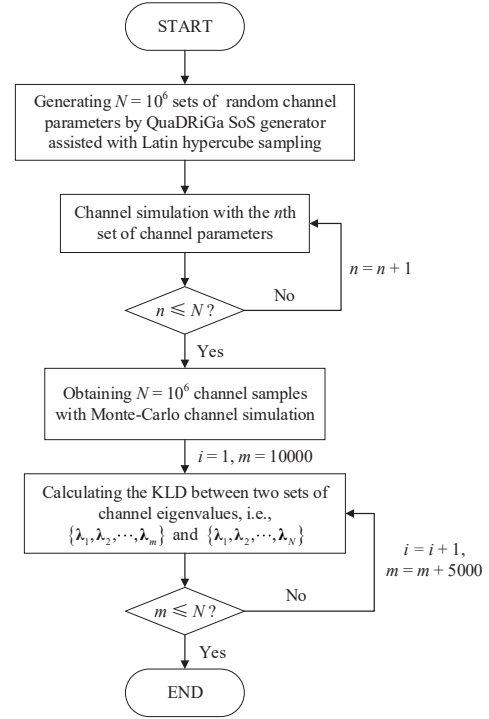


Fig. 3. Flow chart of the ergodicity analysis for a stochastic channel.

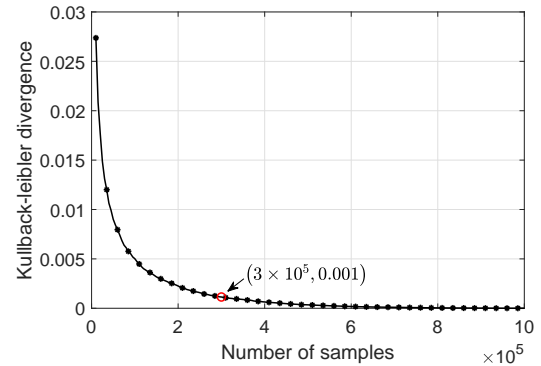


Fig. 4. KLD curve of the channel statistics with respect to sample size.

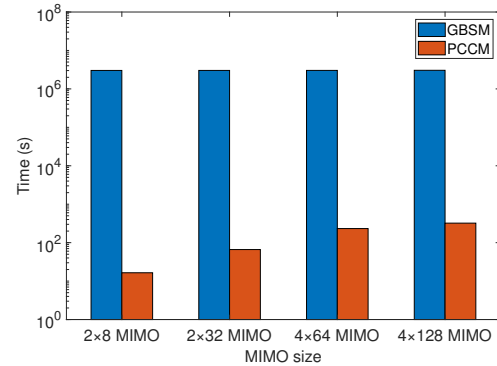


Fig. 5. Comparison of computational complexities between GBSM- and PCCM-based channel simulations.

are omnidirectional and linearly polarized, and the cell is not divided into sectors. To further improve the ergodicity perfor-

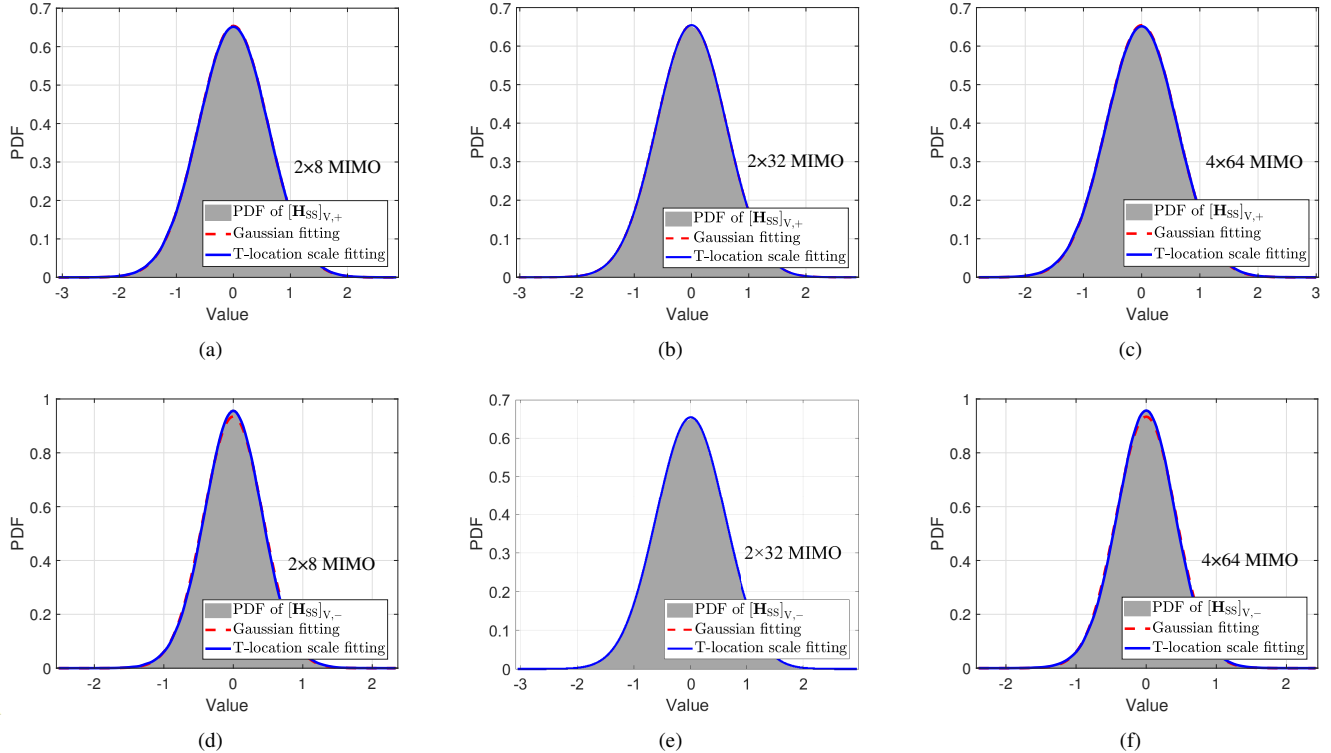


Fig. 6. The distribution fits for the small-scale channel coefficients. (a) (d)  $[\mathbf{H}_{SS}]_{V,+}$  and  $[\mathbf{H}_{SS}]_{V,-}$  of the  $2 \times 8$  MIMO channel; (b) (e)  $[\mathbf{H}_{SS}]_{V,+}$  and  $[\mathbf{H}_{SS}]_{V,-}$  of the  $2 \times 32$  MIMO channel; (c) (f)  $[\mathbf{H}_{SS}]_{V,+}$  and  $[\mathbf{H}_{SS}]_{V,-}$  of the  $4 \times 64$  MIMO channel.

mance, Latin hypercube sampling (LHS) is applied to generate random phases in sum-of sinusoids (SOS) initializations. For clarity, we use the 3D coordinate  $[x, y, z]$  in meters to describe the BS/UE positions, where  $[x, y]$  is the 2D plane coordinate within the cell and  $z$  represents the height.

#### A. Ergodicity analysis of the stochastic channel

To comprehensively study the statistical behavior of the stochastic channel, it is first necessary to analyze the ergodicity of the channel states. With the “3GPP 38.901 UMi NLOS” at 4.8 GHz, an MC simulation is conducted for a single-user downlink over a  $2 \times 4$  MIMO channel. The locations of the BS and UE are fixed at  $[0, 0, 10]$  and  $[0, 100, 1.5]$ , respectively. The BS antenna is a horizontal uniform linear array (ULA) composed of four omni-elements alternating with  $\pm 45^\circ$  polarization, and the UE side uses two vertically polarized (VP) omni-antennas. Both the BS and UE antenna elements are arranged at 1 wavelength interval. During the simulation, both the BS and UE remain stationary, while the scattering environment varies for each channel generation. That is, the channel parameters are randomly initialized according to the distributions specified in the 3GPP TR 38.901. A total of  $10^6$  random channel samples are generated and regarded as the reference ergodic channel states.

The execution flow of the Kullback–Leibler divergence (KLD)-based scheme is presented in Fig. 3. With a proper KLD threshold, one can learn the minimum size of channel samples to simulate that can be traversable as far as possible with the lowest computational cost. Fig. 4 shows the KLD

results calculated between the eigenvalues obtained from the reference ergodic channel samples and the dynamic  $\mathbf{H}$  data set evenly spaced with 5000 samples. The KLD remains below 0.001 with a sample size larger than  $3 \times 10^5$ ; thus, we consider  $3 \times 10^5$  as the proper size of the stochastic channel samples to simulate for further statistical analysis.

#### B. Monte Carlo MIMO channels for fixed user links

A series of MC simulations for the stochastic MIMO channels between a BS and a fixed UE are conducted. By numerical analysis, we focus on the following three problems:

- 1) The performance of the proposed PCCM compared with that of the GBSM and the JCCM (Weichselberger’s model);
- 2) The channel capacities of a single-user link with different MIMO configurations;
- 3) The channel capacities of fixed user links associated with different scenarios and frequencies.

The randomness of the MIMO channel characteristics is reflected in the stochastic multipath scattering, i.e., the NLOS components. To investigate the distribution of the small-scale channel coefficients, without loss of generality, the “3GPP TR 38.901 UMi NLOS” at 4.8 GHz is adopted, and the UE is located at  $[0, 100, 1.5]$  with arbitrary orientations. The BS/UE arrays are configured with four different MIMO scales (i.e.,  $2 \times 8$  MIMO,  $2 \times 32$  MIMO,  $4 \times 64$  MIMO and  $4 \times 128$  MIMO). The 8-element Tx antenna is a horizontal ULA composed of 4 pairs of cocenter elements with  $\pm 45^\circ$  orthogonal polarizations and an interval of 1 wavelength, whereas the 32-element, 64-element and 128-element Tx antennas are uniform planar

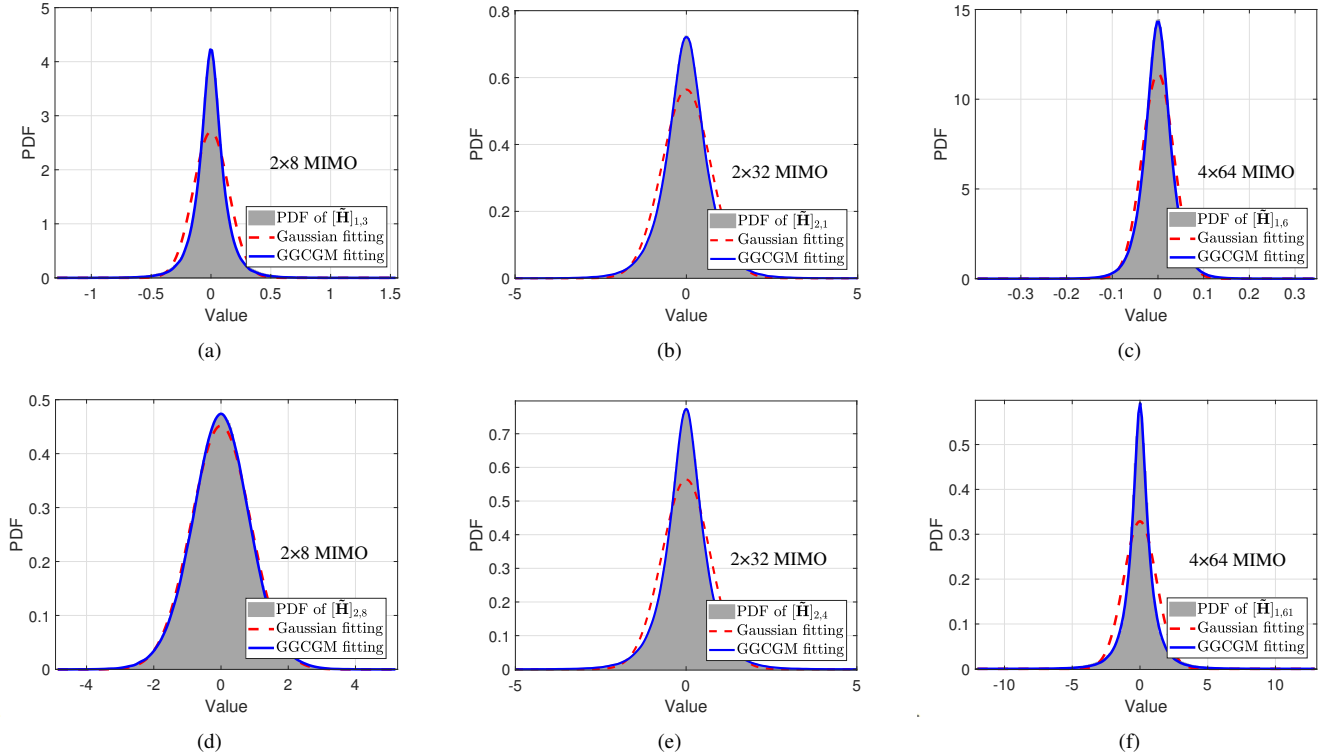


Fig. 7. The distribution fits for the decorrelated channel coefficients. (a) (d)  $[\tilde{\mathbf{H}}]_{1,3}$  and  $[\tilde{\mathbf{H}}]_{2,8}$  of the  $2 \times 8$  MIMO channel; (b) (e)  $[\tilde{\mathbf{H}}]_{2,1}$  and  $[\tilde{\mathbf{H}}]_{2,4}$  of the  $2 \times 32$  MIMO channel; (c) (f)  $[\tilde{\mathbf{H}}]_{1,6}$  and  $[\tilde{\mathbf{H}}]_{1,61}$  of the  $4 \times 64$  MIMO channel.

arrays (UPAs), each consisting of cocenter elements with  $+/-45^\circ$  orthogonal polarizations that are evenly arranged in 4 rows with 0.5 wavelength spacing. The 4-element Rx antenna is composed of  $2 \times 2$  VP omni-antennas with 1 wavelength spacing. For each MIMO configuration, a total of  $3 \times 10^5$  GBSM channel samples are generated.

First, we employed code execution time as a metric for comparison to assess the computational complexity of channel simulations across various MIMO antenna configurations. Utilizing an identical computer configuration featuring an AMD EPYC 7H12 64-Core Processor and 512 GB of memory, we generated 300,000 samples of MIMO channels in configurations of  $2 \times 8$ ,  $2 \times 32$ ,  $4 \times 64$ , and  $4 \times 128$ , employing QuaDRiGa and PCCM codes, respectively, within the MATLAB environment. Fig. 5 presents a comparative bar chart illustrating the average program execution time obtained from 100 repeated simulations. The simulation time for channel simulations based on the GBSM is not substantially influenced by the MIMO scale. This phenomenon is attributed to the fact that the predominant computational consumption in the GBSM occurs during the generation of random channel parameters using the SoS algorithm, for which the number of invocations is associated with the number of clusters and subchannels. Conversely, the computational complexity of the PCCM increases in proportion to the size of the random matrix  $\mathbf{H}_{\text{ind}}$ , which corresponds to the dimensions of the transceiver antenna arrays. Nonetheless, despite this increase, the computational complexity of the channel simulations based on the PCCM remains significantly lower than that based on the GBSM.

For clarity, the subscripts  $V$ ,  $+$  and  $-$  are used to indicate

vertical polarization,  $+45^\circ$  linear polarization and  $-45^\circ$  linear polarization, respectively. For example, the distribution of  $[\mathbf{H}_{\text{SS}}]_{V,+}$  covers the distributions of all the channel coefficients between a VP Rx antenna and a  $+45^\circ$  linearly polarized Tx antenna. As shown in Fig. 6, the R/I components of the  $[\mathbf{H}_{\text{SS}}]_{V,+}$  elements follow an i.i.d. Gaussian distribution, while the others (i.e., the  $[\mathbf{H}_{\text{SS}}]_{V,-}$  elements) obey a T-location scale distribution with positive excess kurtosis. That is, the R/I components of the small-scale channel coefficients are i.i.d. and associated with the antenna polarizations. With decorrelation, as presented in Fig. 7, the independent  $[\tilde{\mathbf{H}}]$  elements show even more freedom in statistics and fit well with the GGCGM distributions with various shapes and scales, which demonstrates the excellent capability of the PCCM in characterizing the practical propagation environment. In addition, the overall gap in statistics between the GBSM and the fitted Gaussian samples becomes larger with an increase in the MIMO scale, which aggravates the drawback of the i.i.d. complex Gaussian  $\mathbf{H}_{\text{iid}}$  (i.e., the  $\mathbf{G}$  matrix)-based JCCM for massive MIMO transmission.

Simulations of a  $2 \times 32$  MIMO channel with UMi/UMa NLOS scenarios at 4.8 GHz are adopted to compare the stochastic MIMO channels in various scenarios. The channel performance is represented by the PDF of the channel capacity and the cumulative probability function (CDF) of the normalized EVs. As shown in Figs. 8 and 9, taking the GBSM results as reference, overestimation of the channel performance may occur based on the classical JCCM, and the gap between the GBSM and JCCM for the UMa NLOS channel is much larger

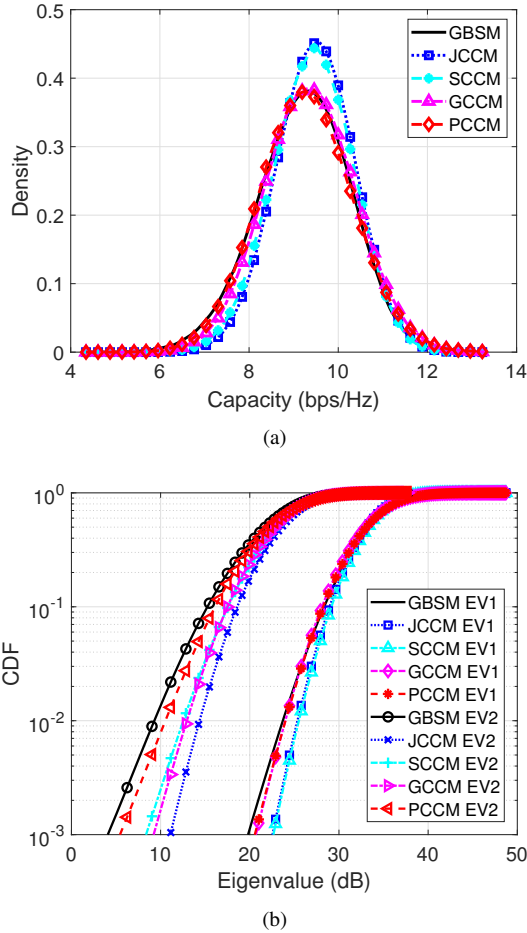


Fig. 8. Comparison of the  $2 \times 32$  UMi NLOS MIMO channel performance among the GBSM, JCCM, SCCM and PCCM. (a) PDFs of the capacity; (b) CDFs of the normalized EVs.

than that in the UMi NLOS case. However, for both scenarios, the PCCM demonstrates significant improvement in statistical accuracy, thereby providing a more reliable channel statistical characterization approach to the high-performance GBSM.

As shown in Figs. 10 and 11, the PCCM also exhibits excellent performance in the massive MIMO channel scenario. The overestimation of the capacity based on the JCCM worsens with increasing MIMO scale. Therefore, the classic JCCM is no longer reliable for massive MIMO channel characterization. In contrast, the proposed PCCM shows perfect statistical approximation to the GBSM with arbitrary MIMO configurations. Furthermore, upon comparing the performance of the GCCM, SCCM and PCCM, it is found that the PCCM achieves the best statistical agreement with the GBSM. The GCCM shows a good statistical fit to the maximum eigenvalue, while there are deviations when fitting other EVs. The SCCM exhibits better performance than the JCCM in scenarios with multiple EVs (i.e.,  $\text{rank}\{\mathbf{H}\} > 2$ ).

The PCCM also showcases its versatility in scenarios featuring nonuniform antenna arrays. In the experiments, we conduct simulations on a MIMO channel with a nonuniform planar array (NUPA) at the BS antenna, wherein the BS antenna elements transition from an initially uniform arrangement with

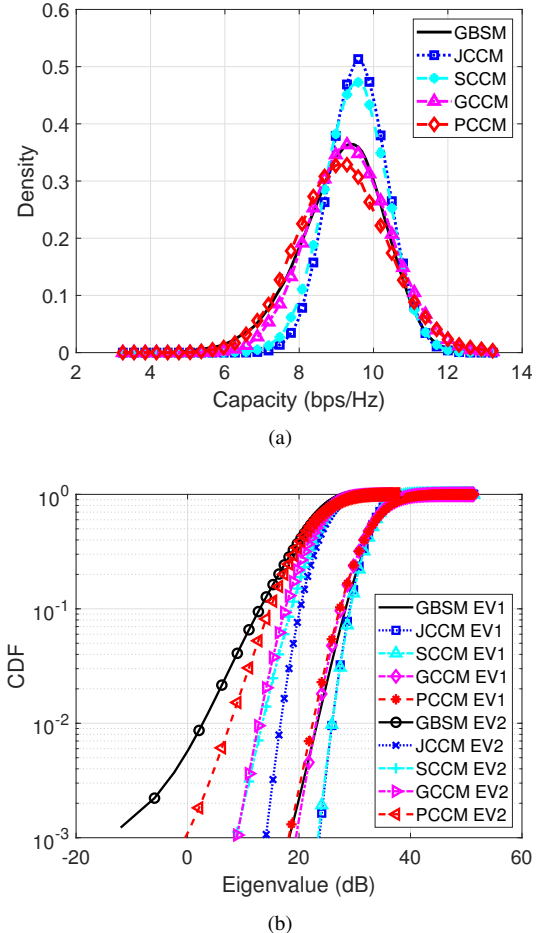


Fig. 9. Comparison of the  $2 \times 32$  UMa NLOS MIMO channel performance among the GBSM, JCCM, SCCM, GCCM and PCCM. (a) PDFs of the capacity; (b) CDFs of the normalized EVs.

0.5-wavelength spacing to random spacing ranging from 0.5 to 1 wavelength. The validation results are presented in Fig. 12.

To investigate the channel performance with respect to frequency, the  $2 \times 32$  MIMO channels with the “3GPP TR 38.901 UMa NLOS” at 4.8 GHz and 26.5 GHz are adopted for simulation. Considering the millimeter wave channel characteristics, only 6 effective clusters (i.e., 1 LOS cluster and 5 NLOS clusters) are generated for each channel realization. Fig. 13 compares the normalized channel capacities estimated from the GBSM, JCCM and PCCM. Due to different numbers of clusters, the channel diversity capability at 26.5 GHz is weaker than that at 4.8 GHz, but the JCCM fails to show this difference. In contrast, the PCCM achieves perfect agreement with the GBSM in terms of channel performance.

The PCCM is also applicable to LOS MIMO channels. For the  $2 \times 32$  MIMO channel and  $4 \times 64$  UMi MIMO channel in the “3GPP TR 38.901 UMi LOS” scenario at 4.8 GHz, the distributions of the normalized channel capacities and EVs are given in Fig. 14 and Fig. 15, respectively. The accuracy of the PCCM is significantly improved compared with that of the classic JCCM.

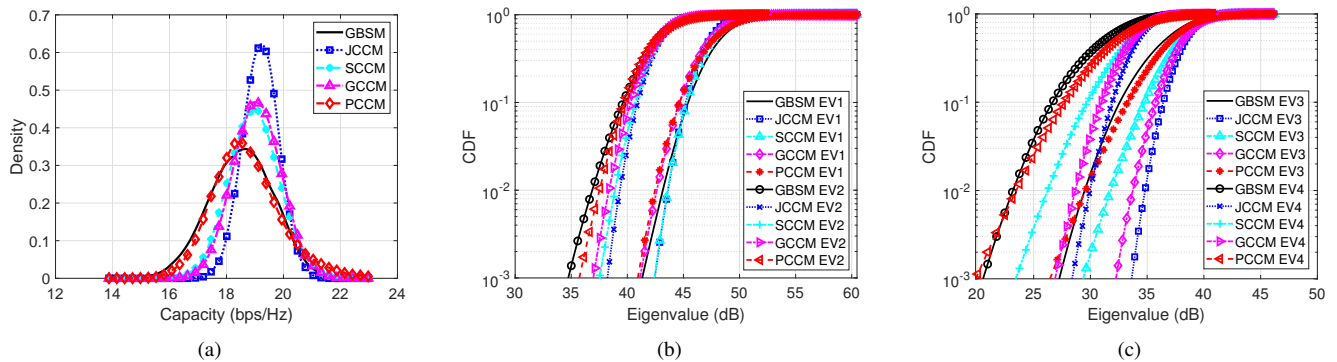


Fig. 10. Comparison of the  $4 \times 128$  UMi NLOS MIMO channel performance among the GBSM, JCCM, SCCM, GCCM and PCCM. (a) PDFs of the capacity; (b)(c) CDFs of the normalized EVs.

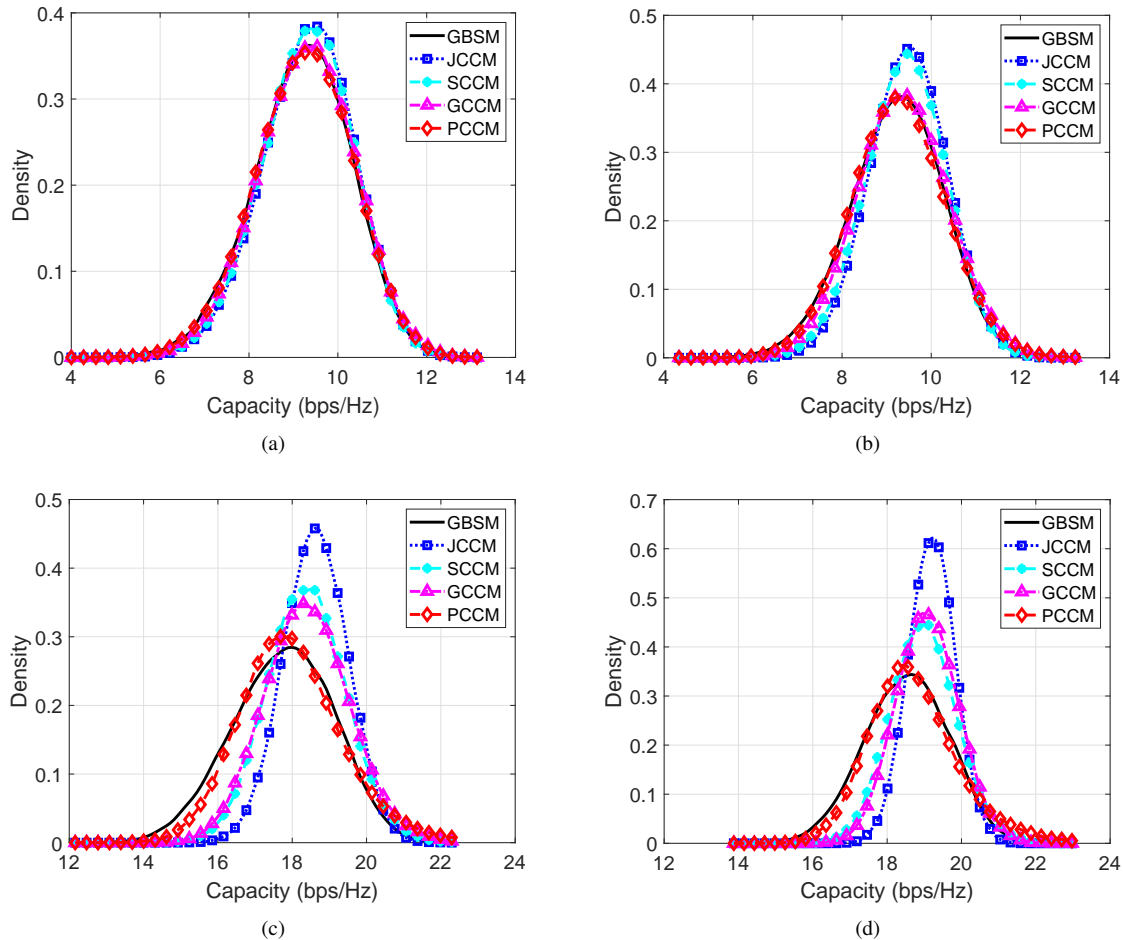


Fig. 11. PDFs of the capacities for UMi NLOS channels with different MIMO scales. (a)  $2 \times 8$  MIMO channel; (b)  $2 \times 32$  MIMO channel; (c)  $4 \times 64$  MIMO channel; (d)  $4 \times 128$  MIMO channel.

### C. Continuous Time Evolution NLOS MIMO channels

Two channel configurations, i.e., a  $2 \times 8$  MIMO channel and  $2 \times 128$  MIMO channel, are adopted for simulation of the continuous time evolution NLOS MIMO channel. The scenario is “3GPP TR 38.901 UMa NLOS” at 4.8 GHz. The UE moves straight eastward at a constant speed of 60 km/h from  $[0, 50, 1.5]$  to  $[0, 150, 1.5]$ . Based on the QuaDRiGa framework, when the UE is moving, the arrival angles, delays and phases are updated using geometric calculations. To ensure

the ergodicity of the channel samples,  $3 \times 10^5$  channel samples are generated over the user track.

For the case of the  $2 \times 8$  UMa NLOS MIMO channel, the distribution fittings for the GBSM  $\mathbf{H}_{SS}$  and  $[\hat{\mathbf{H}}]$  samples are presented in Fig. 17. The  $\mathbf{H}_{SS}$  elements are approximately complex Gaussian distributed, while the i.n.d.  $[\hat{\mathbf{H}}]$  elements deviate from the Gaussian shape due to large kurtosis and fit well with the proposed GGCGM distribution.

The channel statistical properties for the GBSM, JCCM and

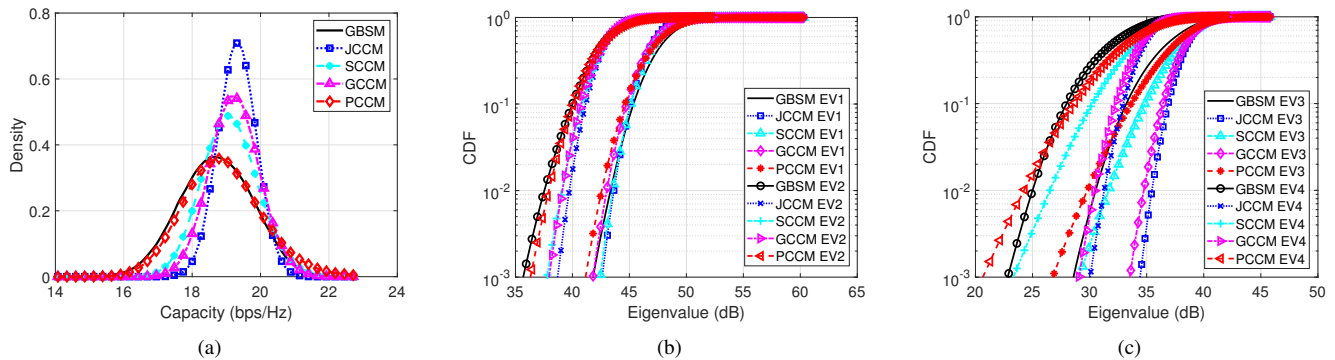


Fig. 12. Comparison of the  $4 \times 128$  UMi NLOS MIMO channel performance with a NUPA BS antenna. (a) PDFs of the capacity; (b)(c) CDFs of the normalized EVs.

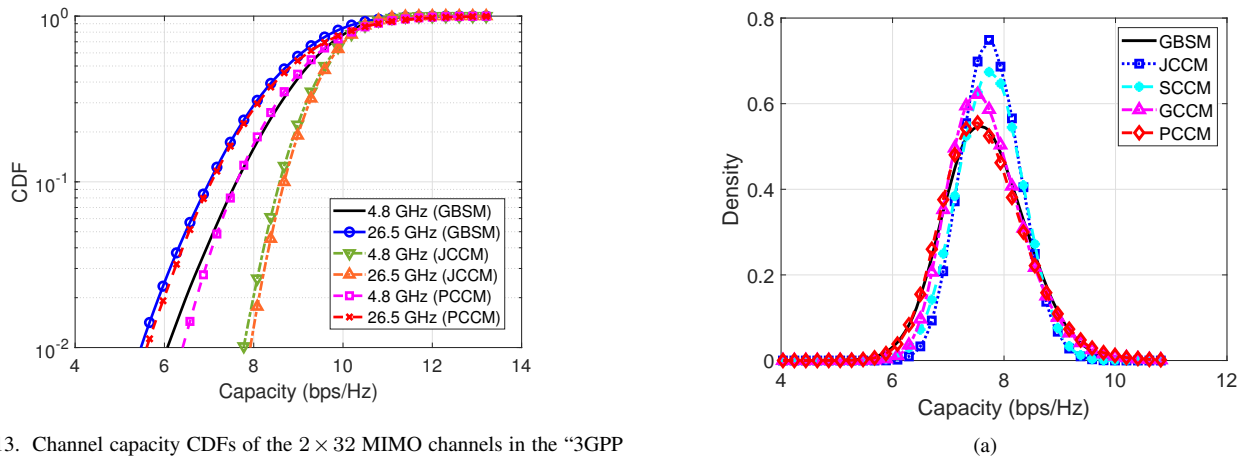


Fig. 13. Channel capacity CDFs of the  $2 \times 32$  MIMO channels in the “3GPP TR 38.901 UMa NLOS” scenario at 4.8 GHz and 26.5 GHz.

PCCM are presented with the corresponding distributions of the channel capacities (SNR = 15 dB) and the EVs in Fig. 18 and Fig. 19. Compared to the JCCM, the PCCM is reliable, with an excellent approximation to the GBSM.

#### D. Cell-based Ergodic NLOS MIMO channels

The cell-based MIMO ergodic channel is defined as the stochastic wireless MIMO channel between the BS and mobile users that drop ergodically in the effective communication area of a cell. Numerical experiments demonstrate that the proposed PCCM is also applicable to characterize cell-based MIMO NLOS channels.

To efficiently traverse the channel states, the simulation is realized based on a spatially correlated multiuser channel. Taking the 3GPP TR 38.901 UMi NLOS scenario, for example, the QuaDRiGa model is developed with the layout shown in Fig. 20, where  $3 \times 10^4$  mobile users evenly drop in the circular open area and move with a constant linear speed and arbitrary orientations. Time evolution channel simulations are performed simultaneously for all user links; accordingly, the “3GPP baseline” is disabled in the QuaDRiGa setup to enable spatial consistency of the channel states. With 10 snapshots per user generated along the user track with a space of a half wavelength,  $3 \times 10^5$  channel samples are acquired in total for the cell-based MIMO channel. On this basis, both

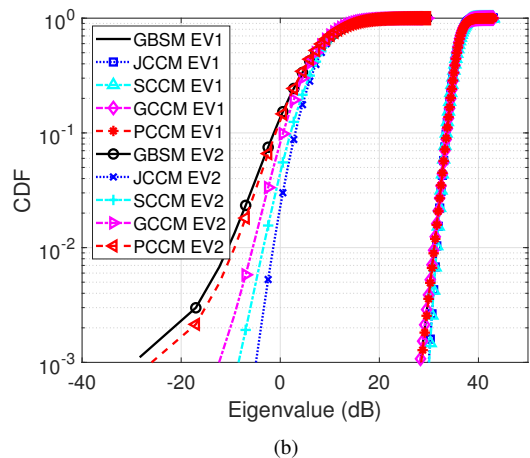
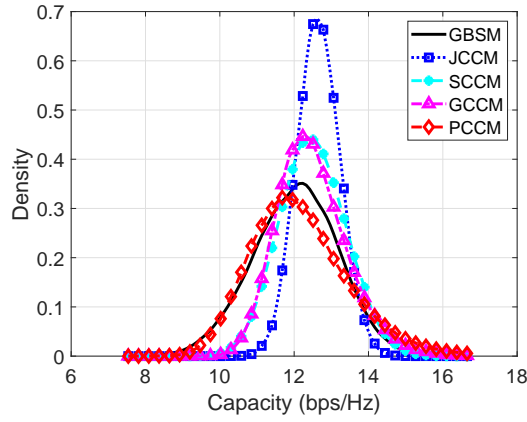


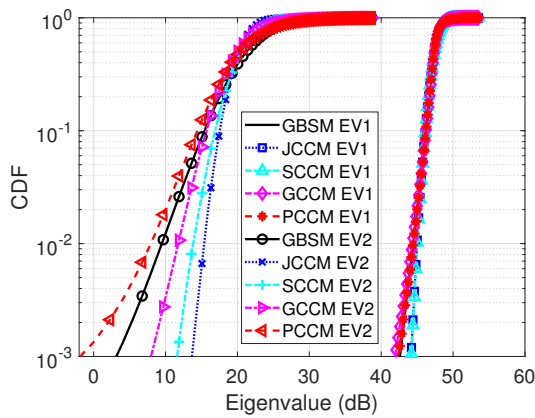
Fig. 14. Comparison of the  $2 \times 32$  UMi LOS MIMO channel performance among the GBSM, JCCM, SCCM, GCCM and PCCM. (a) PDFs of the capacity; (b) CDFs of the normalized EVs.

the JCCM and PCCM are developed for comparative analysis of modeling performance.

Without loss of generality,  $2 \times 8$  and  $2 \times 32$  MIMO antennas are configured at the transceiver ends in the “3GPP TR 38.901 UMi NLOS” and “3GPP TR 38.901 UMa NLOS” scenarios at 4.8 GHz. The UMi/UMa NLOS channel capacities and the EVs generated by the GBSM, JCCM and PCCM are presented in Figs. 21 and 22, respectively. The PCCM achieves a better



(a)



(b)

Fig. 15. Comparison of the  $4 \times 64$  UMi LOS MIMO channel performance among the GBSM, JCCM, SCCM, GCCM and PCCM. (a) PDFs of the capacity; (b) CDFs of the normalized EVs.

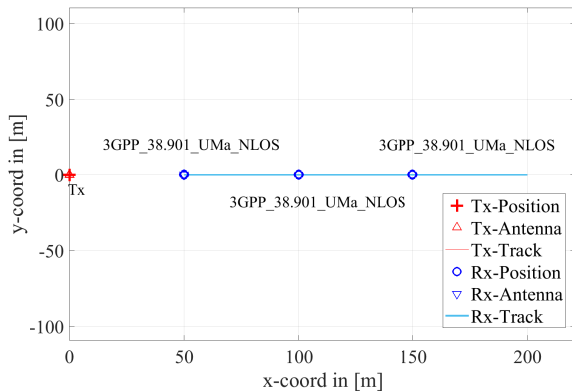
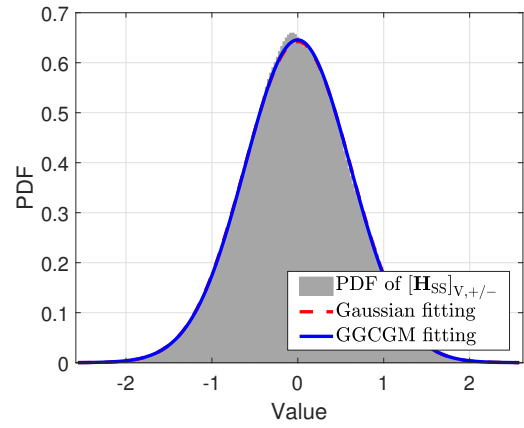


Fig. 16. Layout of the QuaDRiGa model for a moving UE.

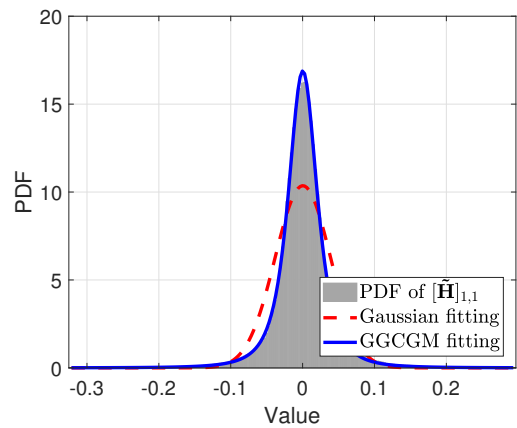
approximation of the statistical channel performance to the 3GPP 38.901 model.

## V. CONCLUSION

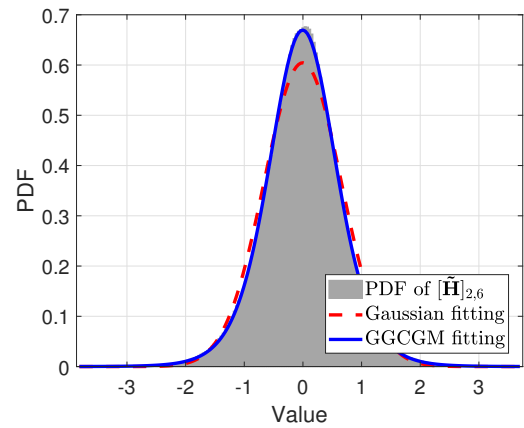
A PCCM for massive MIMO transmission that provides a pervasive expression for representing stochastic MIMO channels with arbitrary MIMO scales and statistical behavior has been proposed. To reduce the model complexity, the GCCM



(a)



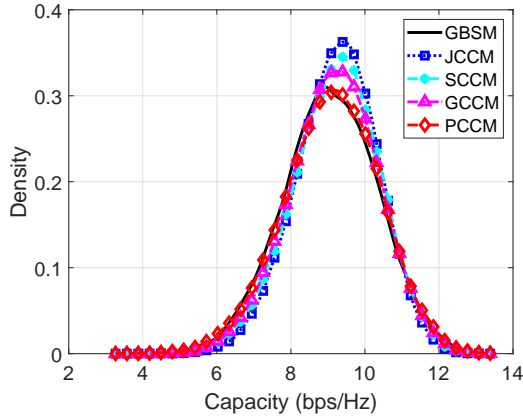
(b)



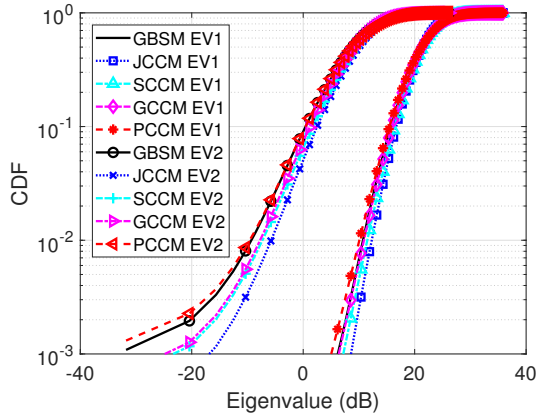
(c)

Fig. 17. The distribution fits for the  $2 \times 8$  time evolution UMa NLOS MIMO channel coefficients. (a)  $[\mathbf{H}_{SS}]_{V,+/-}$ ; (b)  $[\tilde{\mathbf{H}}]_{1,1}$ ; (c)  $[\tilde{\mathbf{H}}]_{2,6}$ .

and SCCM are also addressed as alternatives for application. The statistical properties of the small-scale MIMO channel have been investigated with and without spatial correlations, and a novel mixture distribution named GGCGM is proposed to obtain excellent fitting of the higher-order statistics for each independent subchannel. This approach makes the PCCM capable of reflecting more detailed features of the signal propagation over the air. The elements in the matrix  $\mathbf{R}_{\text{ind}}$  can be



(a)



(b)

Fig. 18. Comparison of the  $2 \times 8$  time evolution UMa NLOS MIMO channel performance among the GBSM, JCCM, SCCM, GCCM and PCCM. (a) PDFs of the capacity; (b) CDFs of the normalized EVs.

arbitrarily distributed by classifying the  $\mathbf{H}_{\text{ind}}$  distributions into three typical categories and quick initialization formulae for the GGCGM feature parameters are provided to adapt different distribution shapes. Numerical results have demonstrated the advantages of the proposed PCCM in accuracy and universality compared to existing CBSMs.

#### APPENDIX A

##### DISTRIBUTION TRANSFORMATION WITH THE SAME CUMULATIVE PROBABILITIES

A Gamma variable  $x \sim \Gamma(\alpha, \beta)$  can be transformed from a Gaussian variable  $y \sim N(\mu, \sigma)$  using the uniformly distributed sequence  $z \sim U(0, 1)$  corresponding to the cumulative probability of  $y$ :

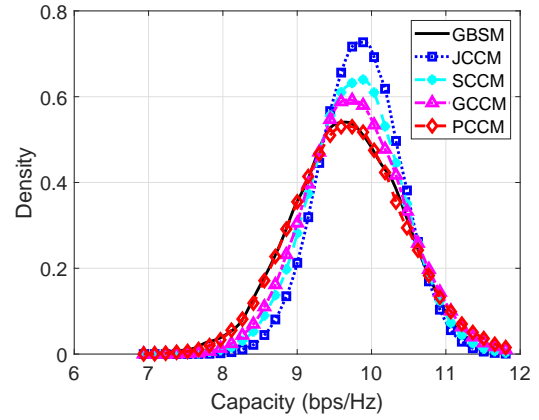
$$z = \text{cdf}(y) = \frac{1}{2} \text{Erfc}\left(-\frac{x - \mu}{\sqrt{2}\sigma}\right), \quad (32)$$

$$x = F_{\Gamma}^{-1}(z|\alpha, \beta) = \{x : F_{\Gamma}(z|\alpha, \beta) = z\}, \quad (33)$$

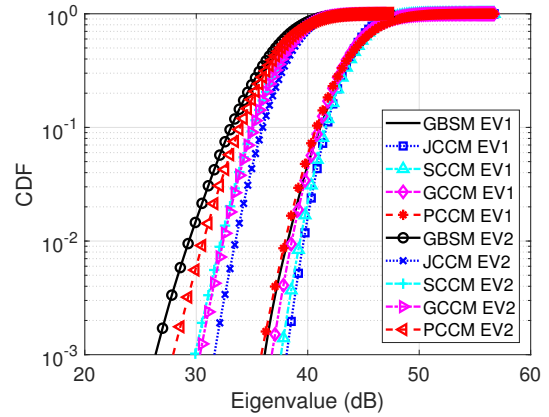
where

$$\text{Erfc}(u) = \frac{2}{\sqrt{\pi}} \int_u^{\infty} e^{-t^2} dt, \quad (34)$$

$$F_{\Gamma}(z|\alpha, \beta) = \frac{1}{\beta^{\alpha}\Gamma(\alpha)} \int_0^z t^{\alpha-1} e^{-\frac{t}{\beta}} dt, \quad z > 0. \quad (35)$$



(a)



(b)

Fig. 19. Comparison of the  $2 \times 128$  time evolution UMa NLOS MIMO channel performance among the GBSM, JCCM, SCCM, GCCM and PCCM. (a) PDFs of the capacity; (b) CDFs of the normalized EVs.

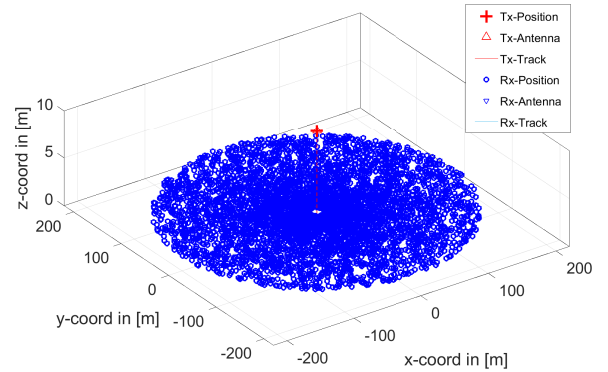


Fig. 20. Layout of the QuadRiGa model of the stochastic MIMO channel with moving users.

Similarly, a Rayleigh variable  $h \sim R(\sigma)$  can be obtained as follows:

$$h = F_{\text{Rayl}}^{-1}(z|\sigma) = \{h : F_{\text{Rayl}}(z|\sigma) = z\} \quad (36)$$

where

$$F_{\text{Rayl}}(z|\sigma) = 1 - e^{-\frac{z^2}{2\sigma^2}}, \quad z > 0. \quad (37)$$

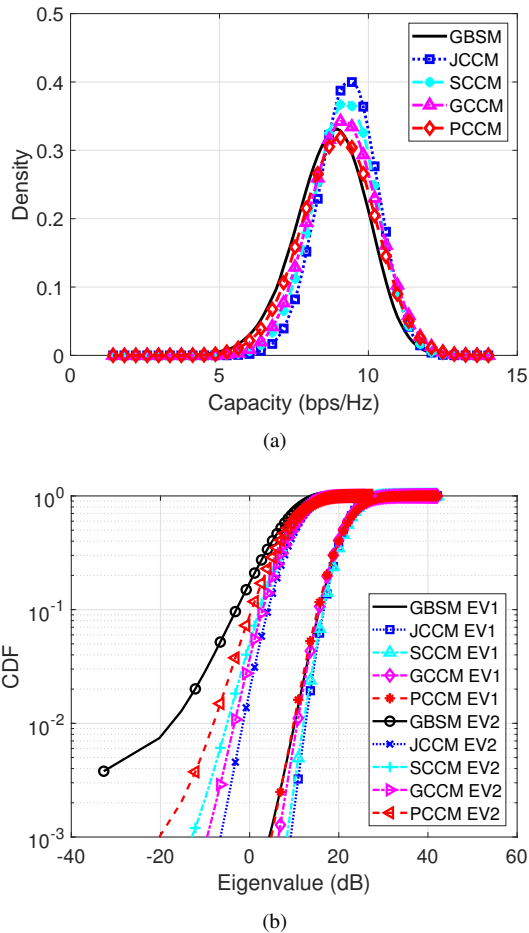


Fig. 21. Comparison of the  $2 \times 8$  cell-based ergodic UMi NLOS MIMO channel performance among the GBSM, JCCM, SCCM, GCCM and PCCM. (a) PDFs of the capacity; (b) CDFs of the normalized EVs.

## APPENDIX B DEFINITION AND PROPERTIES OF THE GGCGM DISTRIBUTION

Here, we briefly outline the definition and statistical properties of the GGCGM distribution proposed in this paper.

The GGCGM variable is defined as the product of a power-generalized Gamma variable and a standard complex Gaussian variable that are independent of each other, i.e.,

$$z = \chi^p (\varepsilon + j\eta) = x + jy \quad (38)$$

where  $\chi$  follows a generalized Gamma distribution,  $\chi^p$  means the  $p$ -th power of an  $\chi$  variable, and  $\varepsilon$  and  $\eta$  are i.i.d. half-varied Gaussian variables,

$$\chi \sim \Gamma(\alpha, \beta, \gamma, \mu). \quad (39)$$

$$\begin{bmatrix} \varepsilon \\ \eta \end{bmatrix} \sim N \left( \begin{bmatrix} 0 \\ 0 \end{bmatrix}, \begin{bmatrix} 1/2 & 0 \\ 0 & 1/2 \end{bmatrix} \right) \quad (40)$$

where  $\alpha, \beta, \gamma, \mu, p$  are constant parameters with  $\alpha > 0, \beta > 0, \gamma > 0$ .

Since the power-generalized Gamma variable and the complex Gaussian variable are independent of each other, the distributions of the R/I components of the GGCGM variable

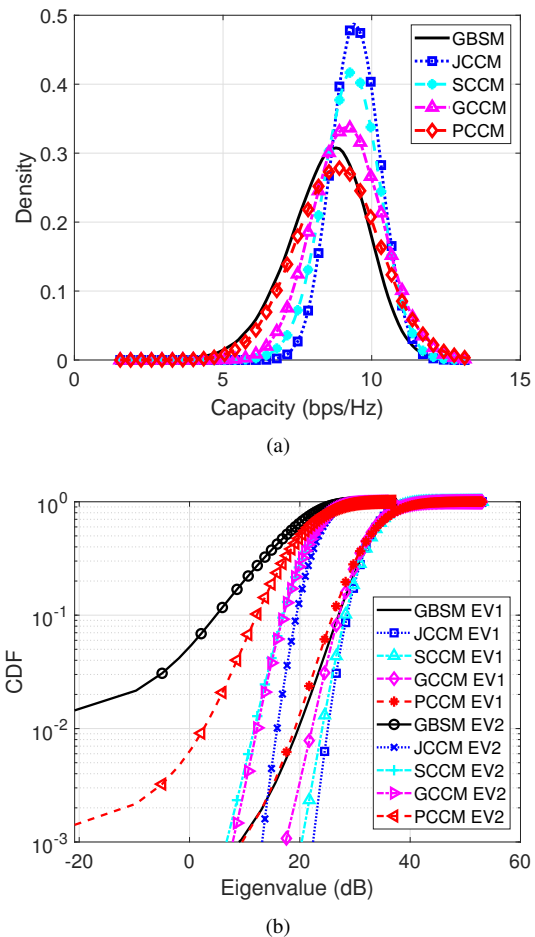


Fig. 22. Comparison of the  $2 \times 32$  cell-based ergodic UMa NLOS MIMO channel performance among the GBSM, JCCM, SCCM, GCCM and PCCM. (a) PDFs of the capacity; (b) CDFs of the normalized EVs.

are identical and both symmetric about zero, and the PDF can be readily estimated by numerical integration:

$$\begin{cases} f(x; \alpha, \beta, \gamma, \mu) = \int_0^\infty \frac{f_{\chi^p}(t)}{t} f_\varepsilon\left(\frac{x}{t}\right) dt \\ f(y; \alpha, \beta, \gamma, \mu) = \int_0^\infty \frac{f_{\chi^p}(t)}{t} f_\eta\left(\frac{y}{t}\right) dt \end{cases} \quad (41)$$

where

$$f_{\chi^p}(v) = \begin{cases} \frac{\gamma \left[ \frac{(v-\mu)^{1/p}}{\beta} \right]^{\alpha\gamma} e^{-\left[ \frac{(v-\mu)^{1/p}}{\beta} \right]^\gamma}}{pv \text{Gamma}(\alpha)}, & v > 0, \\ 0, & \text{else,} \end{cases} \quad (42)$$

$$f_\varepsilon(v) = \frac{1}{\sqrt{\pi}} e^{-v^2}. \quad (43)$$

On the premise that the location feature  $\mu$  is zero, the possible distributions of  $z$  can be roughly classified into three categories. In the first case, as long as  $p = 0$ , the value of  $\chi^p$  is fixed to 1. That is, the GGCGM variable is simplified to a standard complex Gaussian variable.

In the second case, let  $\chi \sim \Gamma(\alpha, \beta, 1, 0)$  and  $p = -1/2$ ; then, the transformed distribution  $z = \chi^{-1/2} (\varepsilon + j\eta)$  is equiv-

alent to a complex Student distribution, i.e.,  $z \sim t(0, \sigma, \nu)$ . The distribution parameters are mapped as follows:

$$\begin{cases} \sigma = \frac{1}{\sqrt{2\alpha\beta}}, \\ \nu = 2\alpha. \end{cases} \quad (44)$$

Otherwise, supposing that  $\chi \sim \Gamma(\alpha, \beta, \gamma, 0)$  and  $p = 1$ , the distribution of  $z$  is close to a complex Laplace shape with higher kurtosis; the shape of  $z$  is dominated by its shape features  $\alpha$  and  $\gamma$ , and the parameters of the distribution can be derived from its statistical features. For example:

$$\begin{cases} M_2 = \frac{\gamma(\alpha + 2/\gamma)\beta^2}{2\gamma(\alpha)}, \\ M_4 = \frac{3\gamma(\alpha + 4/\gamma)\beta^4}{4\gamma(\alpha)}, \\ M_6 = \frac{15\gamma(\alpha + 6/\gamma)\beta^6}{8\gamma(\alpha)}. \end{cases} \quad (45)$$

where  $M_2$ ,  $M_4$  and  $M_6$  are the 2nd, 4th, and 6th moments, respectively, of the R/I component of  $u$ .

## REFERENCES

- [1] J. Winters, J. Salz, and R. Gitlin, "The impact of antenna diversity on the capacity of wireless communication systems," *IEEE Trans. Commun.*, vol. 42, no. 234, pp. 1740–1751, 1994.
- [2] R. Ertel, P. Cardieri, K. Sowerby, T. Rappaport, and J. Reed, "Overview of spatial channel models for antenna array communication systems," *IEEE Pers. Commun.*, vol. 5, no. 1, pp. 10–22, 1998.
- [3] T. Marzetta and B. Hochwald, "Capacity of a mobile multiple-antenna communication link in Rayleigh flat fading," *IEEE Trans. Inf. Theory*, vol. 45, no. 1, pp. 139–157, 1999.
- [4] R. Vaughan and J. Andersen, "Antenna diversity in mobile communications," *IEEE Trans. Veh. Technol.*, vol. 36, no. 4, pp. 149–172, 1987.
- [5] E. G. Larsson, O. Edfors, F. Tufvesson, and T. L. Marzetta, "Massive MIMO for next generation wireless systems," *IEEE Commun. Mag.*, vol. 52, no. 2, pp. 186–195, 2014.
- [6] E. Telatar, "Capacity of multi-antenna Gaussian channels," *Eur. Trans. Telecommun.*, vol. 10, no. 6, pp. 585–595, 1999.
- [7] G. J. Foschini and M. J. Gans, "On limits of wireless communications in a fading environment when using multiple antennas," *Wirel. Pers. Commun.*, 1998.
- [8] H. Bolcskei, D. Gesbert, and A. Paulraj, "On the capacity of OFDM-based spatial multiplexing systems," *IEEE Trans. Commun.*, vol. 50, no. 2, pp. 225–234, 2002.
- [9] J. Garg, K. Gupta, and P. K. Ghosh, "Performance analysis of MIMO wireless communications over fading channels - a review," *Int. J. Adv. Res. in Electr. Electron. & Instrum. Eng.*, vol. 2, no. 4, 2013.
- [10] D. shan Shiu, G. J. Foschini, M. J. Gans, and J. M. Kahn, "Fading correlation and its effect on the capacity of multielement antenna systems," *IEEE Trans. Commun.*, vol. 48, pp. 502–513, 2000.
- [11] Y. Li, X. Cheng, and N. Zhang, "Deterministic and stochastic simulators for non-isotropic V2V-MIMO wideband channels," *China Commun.*, vol. 15, no. 7, pp. 18–29, 2018.
- [12] C. Xiao, Y. R. Zheng, and N. C. Beaulieu, "Novel sum-of-Sinusoids simulation models for Rayleigh and Rician fading channels," *IEEE Trans. Wirel. Commun.*, vol. 5, no. 12, pp. 3667–3679, 2006.
- [13] Y. Yuan, C.-X. Wang, Y. He, M. M. Alwakeel, and e.-H. M. Aggoune, "3d wideband non-stationary geometry-based stochastic models for non-isotropic MIMO vehicle-to-vehicle channels," *IEEE Trans. Wirel. Commun.*, vol. 14, no. 12, pp. 6883–6895, 2015.
- [14] A. G. Zajic and G. L. Stuber, "Three-dimensional modeling and simulation of wideband MIMO mobile-to-mobile channels," *IEEE Trans. Wirel. Commun.*, vol. 8, no. 3, pp. 1260–1275, 2009.
- [15] X. Yin and X. Cheng, "Geometry-based stochastic channel modeling," in *Propagation Channel Characterization, Parameter Estimation, and Modeling for Wireless Communications*. Wiley-IEEE Press, 2016, ch. 4, pp. 77–105.
- [16] K. Anusuya, S. Bharadhwaj, and S. S. Rani, "Wireless channel models for indoor environments," *Defence Science Journal*, vol. 58, no. 6, 2008.
- [17] T. Eyceoz, A. Duel-Hallen, and H. Hallen, "Deterministic channel modeling and long range prediction of fast fading mobile radio channels," *IEEE Commun. Lett.*, vol. 2, no. 9, pp. 254–256, 1998.
- [18] J. Huang, C.-X. Wang, Y. Liu, J. Sun, and W. Zhang, "A novel 3D GBSM for mmWave MIMO channels," *Sci. China-Inf. Sci.*, vol. 61, no. 10, pp. 1–15, 2018.
- [19] C.-X. Wang, X. Cheng, and D. I. Laurenson, "Vehicle-to-vehicle channel modeling and measurements: Recent advances and future challenges," *IEEE Commun. Mag.*, vol. 47, no. 11, pp. 96–103, 2009.
- [20] C.-X. Wang, J. Huang, H. Wang, X. Gao, X. You, and Y. Hao, "6G wireless channel measurements and models: Trends and challenges," *IEEE Veh. Technol. Mag.*, vol. 15, no. 4, pp. 22–32, 2020.
- [21] F. Lai, C.-X. Wang, J. Huang, X. Gao, and F.-C. Zheng, "A novel massive MIMO beam domain channel model," in *2020 IEEE Wireless Communications and Networking Conference (WCNC)*, 2020, pp. 1–6.
- [22] D. S. Baum, J. Hansen, J. Salo, G. Del Galdo, M. Milojevic, and P. Kyösti, "An interim channel model for beyond-3G systems: extending the 3GPP spatial channel model (SCM)," in *2005 IEEE 61st Vehicular Technology Conference*, vol. 5. IEEE, 2005, pp. 3132–3136.
- [23] M. Dotling, W. Mohr, and A. Osseiran, *WINNER II Channel Models*, 2010, pp. 39–92.
- [24] J. Kermaol, L. Schumacher, K. Pedersen, P. Mogensen, and F. Frederiksen, "A stochastic MIMO radio channel model with experimental validation," *IEEE J. Sel. Areas Commun.*, vol. 20, no. 6, pp. 1211–1226, 2002.
- [25] K. I. Pedersen, J. B. Andersen, J. P. Kermaol, and P. Mogensen, "A stochastic multiple-input-multiple-output radio channel model for evaluation of space-time coding algorithms," in *Vehicular Technology Conference Fall 2000. IEEE VTS Fall VTC2000. 52nd Vehicular Technology Conference (Cat. No. 00CH37152)*, vol. 2. IEEE, 2000, pp. 893–897.
- [26] C. Wang, X. Hong, H. Wu, and W. Xu, "A comparative study on the spatial correlation characteristics of the 3GPP spatial channel model and the Kronecker MIMO channel model," in *7th World Wireless Congress*, 2006, pp. 239–244.
- [27] S. Wu, C.-X. Wang, E.-H. M. Aggoune, and M. M. Alwakeel, "A novel kronecker-based stochastic model for massive MIMO channels," in *2015 IEEE/CIC International Conference on Communications in China (ICCC)*. IEEE, 2015, pp. 1–6.
- [28] C.-X. Wang, X. Hong, H. Wu, and W. Xu, "Spatial-temporal correlation properties of the 3GPP spatial channel model and the Kronecker MIMO channel model," *EURASIP J. Wirel. Commun. Netw.*, vol. 2007, pp. 1–9, 2007.
- [29] A. M. Sayeed, "Deconstructing multiantenna fading channels," *IEEE Trans. Signal Process.*, vol. 50, no. 10, pp. 2563–2579, 2002.
- [30] W. Weichselberger, M. Herdin, H. Ozelik, and E. Bonek, "A stochastic MIMO channel model with joint correlation of both link ends," *IEEE Trans. Wirel. Commun.*, vol. 5, no. 1, pp. 90–100, 2006.
- [31] X. Gao, B. Jiang, X. Li, A. B. Gershman, and M. R. McKay, "Statistical eigenmode transmission over jointly correlated MIMO channels," *IEEE Trans. Inf. Theory*, vol. 55, no. 8, pp. 3735–3750, 2009.
- [32] W. Kim, "Distribution of eigenvalues for 2x2 MIMO channel capacity based on indoor measurements," *IEEE Trans. Wirel. Commun.*, vol. 11, no. 4, pp. 1255–1259, 2012.
- [33] W. Kim, H. Lee, J. J. Park, M.-D. Kim, and H. K. Chung, "Modeling of eigenvalues for MIMO channel capacity based on outdoor measurements," in *VTC Spring 2009 - IEEE 69th Vehicular Technology Conference*, 2009, pp. 1–5.
- [34] C. Sun, X. Gao, S. Jin, M. Matthaiou, Z. Ding, and C. Xiao, "Beam division multiple access transmission for massive MIMO communications," *IEEE Trans. Commun.*, vol. 63, no. 6, pp. 2170–2184, 2015.
- [35] 3rd Generation Partnership Project (3GPP), "Study on channel model for frequencies from 0.5 to 100 GHz (Release 17)," Technical Report 3GPP TR 38.901, 2022. [Online]. Available: [https://www.3gpp.org/ftp/Specs/archive/38\\_series/38.901/](https://www.3gpp.org/ftp/Specs/archive/38_series/38.901/)

Min Wang

Yaping He



**Haiming Wang** (M'08) was born in 1975. He received the B.S., M.S., and Ph.D. degrees in Electrical Engineering from Southeast University, Nanjing, China, in 1999, 2002, and 2009, respectively.

He joined the School of Information Science and Engineering, Southeast University, Nanjing, China, in 2002, and is currently a distinguished professor. He is also a part-time professor with the Purple Mountain Laboratories, Nanjing, China. He has authored and co-authored over 50 technical publications in IEEE TRANSACTIONS ON ANTENNAS

AND PROPAGATION and other peer-reviewed academic journals. Prof. Wang has authored and co-authored over more than 70 patents and 52 patents have been granted. He was awarded twice for contributing to the development of IEEE 802.11aj by the IEEE Standards Association in 2018 and 2020.

His current research interests include AI-powered antenna and radio-frequency technologies (iART), AI-powered channel measurement and modeling technologies (iCHAMM), and integrated communications, sensing, and positioning (iCSAP).



**Cheng-Xiang Wang** (S'01-M'05-SM'08-F'17) received the BSc and MEng degrees in Communication and Information Systems from Shandong University, China, in 1997 and 2000, respectively, and the PhD degree in Wireless Communications from Aalborg University, Denmark, in 2004.

He was a Research Assistant with the Hamburg University of Technology, Hamburg, Germany, from 2000 to 2001, a Visiting Researcher with Siemens AG Mobile Phones, Munich, Germany, in 2004, and a Research Fellow with the University of Agder,

Grimstad, Norway, from 2001 to 2005. He has been with Heriot-Watt University, Edinburgh, U.K., since 2005, where he was promoted to a Professor in 2011. In 2018, he joined Southeast University, China, as a Professor. He is also a part-time professor with the Purple Mountain Laboratories, Nanjing, China. He has authored four books, three book chapters, and more than 410 papers in refereed journals and conference proceedings, including 24 Highly Cited Papers. He has also delivered 22 Invited Keynote Speeches/Talks and 7 Tutorials in international conferences. His current research interests include wireless channel measurements and modeling, 6G wireless communication networks, and applying artificial intelligence to wireless communication networks.

Prof. Wang is a Member of the Academia Europaea (The Academy of Europe), a fellow of the IET, an IEEE Communications Society Distinguished Lecturer in 2019 and 2020, and a Highly-Cited Researcher recognized by Clarivate Analytics, in 2017-2020. He is currently an Executive Editorial Committee member for the IEEE TRANSACTIONS ON WIRELESS COMMUNICATIONS. He has served as an Editor for nine international journals, including the IEEE TRANSACTIONS ON WIRELESS COMMUNICATIONS from 2007 to 2009, the IEEE TRANSACTIONS ON VEHICULAR TECHNOLOGY from 2011 to 2017, and the IEEE TRANSACTIONS ON COMMUNICATIONS from 2015 to 2017. He was a Guest Editor for the IEEE JOURNAL ON SELECTED AREAS IN COMMUNICATIONS, Special Issue on Vehicular Communications and Networks (Lead Guest Editor), Special Issue on Spectrum and Energy Efficient Design of Wireless Communication Networks, and Special Issue on Airborne Communication Networks. He was also a Guest Editor for the IEEE TRANSACTIONS ON BIG DATA, Special Issue on Wireless Big Data, and is a Guest Editor for the IEEE TRANSACTIONS ON COGNITIVE COMMUNICATIONS AND NETWORKING, Special Issue on Intelligent Resource Management for 5G and Beyond. He has served as a TPC Member, TPC Chair, and General Chair for over 80 international conferences. He received twelve Best Paper Awards from IEEE GLOBECOM 2010, IEEE ICCT 2011, ITST 2012, IEEE VTC 2013-Spring, IWCMC 2015, IWCMC 2016, IEEE/CIC ICC 2016, WPMC 2016, WOCC 2019, IWCMC 2020, and WCSP 2020.



**Xiaohu You** (Fellow, IEEE) received his M.S. and Ph.D. degrees from Southeast University, Nanjing, China, in Electrical Engineering in 1985 and 1988, respectively.

Since 1990, he has been working with the National Mobile Communications Research Laboratory, Southeast University, where he is currently a Professor and the Director of the National Mobile Communications Research Laboratory. He has contributed over 100 IEEE journal articles and three books in the areas of adaptive signal processing,

neural networks, and wireless communications. His current research interests include wireless networks, advanced signal processing, and its applications. He was a recipient of the National First Class Invention Prize in 2011. He has won the IET Achievement Medal in 2021. He served as the General Chair for the IEEE Wireless Communications and Networking Conference (WCNC) 2013, the IEEE Vehicular Technology Conference (VTC) 2016 Spring, and the IEEE International Conference on Communications (ICC) 2019. From 1999 to 2002, he was the Principal Expert of the C3G Project. From 2001 to 2006, he was the Principal Expert of the China National 863 Beyond 3G FuTURE Project. From 2013 to 2019, he was the Principal Investigator of the China National 863 5G Project. He is currently the Secretary General of the FuTURE Forum, and the Vice Chair of the China IMT-2020 (5G) Promotion Group and the China National Mega Project on New Generation Mobile Networks.